Cell

Engineering source-sink relations by prime editing confers heat-stress resilience in tomato and rice

Graphical abstract

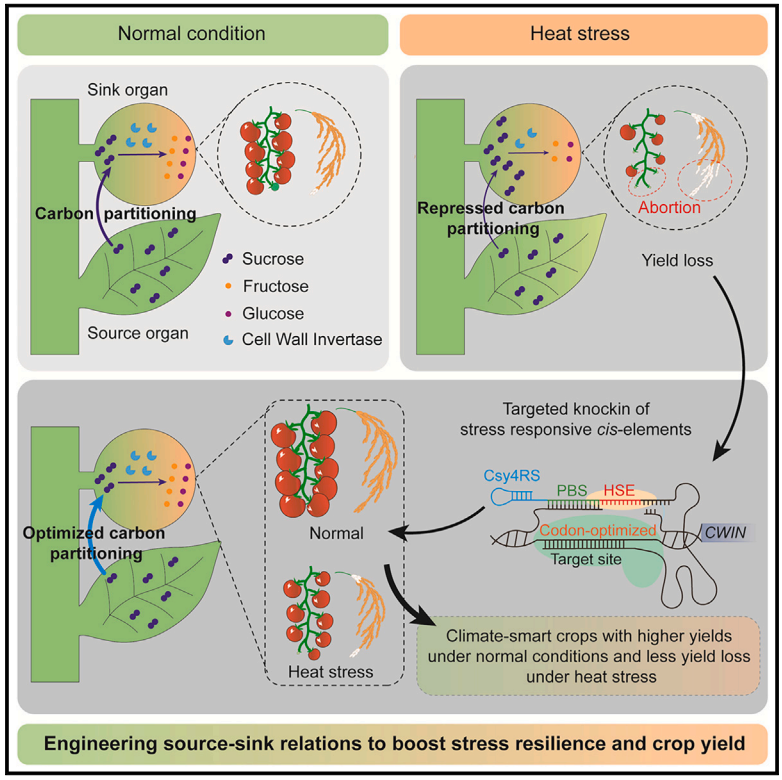

Highlights

- Develop a Csy4-based prime-editing system for efficient, targeted insertion in dicots
- Knockin of heat-shock element confers reactive expression to cell-wall-invertase genes
- Engineer source-sink relations and carbon partitioning to create climate-smart crops
- Lift yield in normal conditions and rescue losses under heat stress in rice and tomato

Authors

Huanchang Lou, Shujia Li, Zihang Shi, ..., Yongfang Yang, Zuoyao Li, Cao Xu

Correspondence

caoxu@genetics.ac.cn

In brief

Lou et al. engineered source-sink relations to improve carbon partitioning by targeted insertion of heat-shock *cis*-elements into cell-wall-invertase genes using prime editing. This delivers climate-smart crops with higher yields under normal conditions and stable yields under heat stress in tomato and rice.

Lou et al., 2025, Cell *188*, 1–20
January 23, 2025
https://doi.org/10.1016/j.cell.2024.11.005

CellPress

Please cite this article in press as: Lou et al., Engineering source-sink relations by prime editing confers heat-stress resilience in tomato and rice, Cell (2025), https://doi.org/10.1016/j.cell.2024.11.005

Cell

CellPress

Article

Engineering source-sink relations by prime editing confers heat-stress resilience in tomato and rice

Huanchang Lou,[1,2,3,5] Shujia Li,[1,2,5] Zihang Shi,[1,2] Yupan Zou,[1,2] Yueqin Zhang,[1,6] Xiaozhen Huang,[1,2] Dandan Yang,[1,2] Yongfang Yang,[1,2] Zuoyao Li,[4] and Cao Xu[1,2,3,7,*]

[1]Key Laboratory of Seed Innovation, National Center for Plant Gene Research (Beijing), Institute of Genetics and Developmental Biology, Chinese Academy of Sciences, Beijing 100101, China

[2]CAS–JIC Centre of Excellence for Plant and Microbial Science, Institute of Genetics and Developmental Biology, Chinese Academy of Sciences, Beijing 100101, China

[3]College of Advanced Agricultural Sciences, University of Chinese Academy of Sciences, Beijing 100049, China

[4]College of Tropical Crops, Hainan University, Haikou, Hainan 570228, China

[5]These authors contributed equally

[6]Present address: College of Coastal Agricultural Sciences, Guangdong Ocean University, Zhanjiang 524088, China

[7]Lead contact

*Correspondence: caoxu@genetics.ac.cn

https://doi.org/10.1016/j.cell.2024.11.005

SUMMARY

A 2°C climate-warming scenario is expected to further exacerbate average crop losses by 3%–13%, yet few heat-tolerant staple-crop varieties are available toward meeting future food demands. Here, we develop high-efficiency prime-editing tools to precisely knockin a 10-bp heat-shock element (HSE) into promoters of cell-wall-invertase genes (*CWINs*) in elite rice and tomato cultivars. HSE insertion endows *CWINs* with heat-responsive upregulation in both controlled and field environments to enhance carbon partitioning to grain and fruits, resulting in per-plot yield increases of 25% in rice cultivar Zhonghua11 and 33% in tomato cultivar Ailsa Craig over heat-stressed controls, without fruit quality penalties. Up to 41% of heat-induced grain losses were rescued in rice. Beyond a prime-editing system for tweaking gene expression by efficiently delivering bespoke changes into crop genomes, we demonstrate broad and robust utility for targeted knockin of *cis*-regulatory elements to optimize source-sink relations and boost crop climate resilience.

INTRODUCTION

Global crop production will need to double by 2050 to meet demand from population growth, dietary changes, and increased biofuel consumption.[1] However, current crop production is insufficient and is expected to worsen from the abiotic-stress burden of climate change.[2,3] An increase of 2°C in the growing season will result in a yield loss of 3%–13%.[4,5] The need to rapidly develop "climate-smart" crops that can achieve higher yields under normal conditions and stable yield under heat stress is urgent for global food security, and breeding bottlenecks remain.[6–8] Optimizing internal nutrient allocation holds significant potential for improving crop yields.[9,10] However, most efforts have primarily focused on cultivation management, whereas rational design and molecular manipulation of nutrient allocation have been challenging.[11]

The fundamental plant physiology concept of source-sink relations was first proposed by Mason and Maskell in 1928 to explain how a limited supply of resources are allocated within plants.[12] Source tissues are net producers of photoassimilates—primarily carbohydrates such as sucrose—whereas sink tissues are net importers using or storing photoassimilates. Sucrose is the major carbon assimilate from photosynthesis and, together with hydrogen and oxygen in multiple forms, constitutes ~90% of plant biomass and is a crucial yield determinant.[13,14] Sucrose is transported from source tissues through the phloem to sink tissues, wherein it is degraded into hexose or its derivatives, primarily glucose and fructose, to support the growth of sinks, such as roots, developing flowers, fruits, seeds, cotton fibers, and storage organs.[11,15] Sucrose is degraded by either invertases into glucose and fructose or by sucrose synthases (SuSy) into uridine diphosphoglucose and fructose.[9]

Invertases form two broad classes: the acid invertases, which include cell-wall invertases (CWINs) and vacuolar invertases (VINs), and neutral/alkaline cytosolic invertases (CIN), which localize to the cytoplasm.[16,17] CWINs play indispensable roles in providing nutrients, energy sources, and signaling molecules for plant growth, yield, and stress responses.[11] *CWIN* genes have been selected during the domestication of major crops, including tomato[18,19] and rice.[20] *LIN5*, a tomato *CWIN*, was mapped to a major quantitative trait locus determining fruit-sugar level and yield.[21] Tomato varieties containing a *LIN5* allele from the wild relative *Solanum pennellii* with a single-nucleotide polymorphism near the catalytic site have higher sugar contents

Please cite this article in press as: Lou et al., Engineering source-sink relations by prime editing confers heat-stress resilience in tomato and rice, Cell (2025), https://doi.org/10.1016/j.cell.2024.11.005

in fruits, whereas knockdown of *LIN5* produces stunted seeds and fruits with a high frequency of abortion.[21,22] In maize, loss of function of *MINIATURE 1* (*Mn1*), the ortholog of *LIN5*, results in a classical miniature-seed phenotype and about a 70% reduction in grain yield.[23] Rice *GRAIN INCOMPLETE FILLING 1* (*GIF1*) encodes a CWIN ortholog of LIN5 and Mn1 that controls photoassimilate partitioning during early grain filling and determines final grain yield, the regulatory region of which most likely was selected during domestication.[20]

The physiological basis of heat-induced yield and quality reduction is that source-sink balance is disrupted, resulting in inadequate energy supply in sink organs, reduced reproductive development, and yield penalties.[24–26] Heat stress rapidly represses carbon partitioning into sink organs and causes selective abortion of grains or ovaries, a widespread problem and major cause of yield losses in cereal and fruit crops.[17,27] This "strategic abandonment" type of trade-off enables plants to adapt to changing environments when nutrients are insufficient.[10,28] This sensitivity has been retained during crop domestication but is undesirable in agricultural ecosystems in the context of climate change. Relatively little effort has focused on optimizing environmentally sensitive plant-metabolic processes, especially toward uncoupling repression of carbon partitioning because this has practically never been overtly selected.[29] Ectopic expression of *CWINs* has been attempted to enhance carbon partitioning efficiency but often fails and is typically accompanied by yield penalties,[20,30,31] suggesting the importance of fine-tuning source-sink relationships.

Reproductive development of many crops, including tomato, rice, and grain legumes, is more sensitive to higher temperatures at night than daytime temperatures.[32,33] For example, up to 80% of tomato flowers or fruits abort when nighttime temperatures exceed 24°C.[13] This suggests that the insufficient supply of carbon assimilates to sink organs at night can exacerbate the effects of heat stress. Unfortunately, greater nighttime warming is now more prevalent globally compared with daytime warming.[34] To address the threat of climate change to crop yields and the urgent need for rapid plant breeding, we improved prime-editing tools to develop a climate-responsive optimization of carbon partitioning to sinks (CROCS) strategy by rationally manipulating the expression of *CWINs* in fruit and cereal crops.

RESULTS

Heat-stress-induced repression of invertase-dependent carbon partitioning causes tomato yield loss

To explore the quality and yield penalties from heat stress in tomato, we cataloged phenotypes of the table-tomato and model cultivar Ailsa Craig in the greenhouse and monitored temperature from 5-days post anthesis (DPA) (Figures S1A and S1B). Long-term (30-days) heat stress with average day/night temperatures of 32°C/25°C caused a 48% decrease in fruit-setting rate (Figures S1C and S1D), a 63% reduction in fruit fresh weight (Figure S1E), and an 80% loss of fruit yield (Figure S1F), Brix content, a parameter reflecting tomato quality, was reduced by 9% (Figure S1G). We then investigated the impact of short-term acute heat stress on fruit yield. Penalties were replicated in a growth chamber following a short-term (14-days) exposure to 40°C/30°C day/night temperatures. Heat-stressed tomato plants produce small and aborted fruits (Figures 1A–1C), with a 35% decrease in fruit set, a 42% reduction in fruit fresh weight, and a 50% yield loss with reduction in Brix content (Figures 1D–1G).

We then tracked at high resolution how fruit development responds to heat stress by using the dwarf tomato variety Micro-Tom in the growth chamber, which showed similar fruit-set and yield loss effects to Ailsa Craig under heat stress (Figures S1H–S1L). From 5–30 DPA, high temperatures resulted in fruit de-greening and delayed development (Figure 1H), and stunting occurred from 20 DPA (Figure 1I). A remarkable decline in fruit size started at 15 days after the onset of stress treatment (Figures 1H and 1I). Impaired fruit development prompted us to examine sink activity. Sucrose content in heat-stressed fruits was approximately 8-fold higher than fruits grown under normal conditions (Figure 1J); however, glucose and fructose showed dramatic decreases in heat-treated fruits (Figures 1K and 1L). This phenomenon similarly occurred in Ailsa Craig (Figures S1M–S1O). These results indicated that invertase activity was inhibited and developing fruits became hexose deficient. Consistently, the CWIN gene *LIN5* was downregulated under heat stress (Figures 1M and S1P). By contrast, other key factors for partitioning sucrose or starch to sink organs, including tomato *SUCROSE SYNTHASE* (*SlSUS*), *SUCROSE TRANSPORTER 1* (*SlSUT1*), *SUCROSE PHOSPHATE SYNTHASE* (*SlSPS*), and *GLUCAN WATER-DIKINASE* 1 (*SlGWD1*),[35–38] were not repressed by heat stress (Figure S1Q).

We used CRISPR-Cas9 to generate *LIN5* loss-of-function mutants ($lin5^{CR}$) in Micro-Tom background (Figure S1R). The $lin5^{CR}$ mutants were stunted throughout development, showing reduced height and smaller fruit and leaves (Figures 2A–2D). Yield per plant and fruit fresh weight in $lin5^{CR}$ mutants decreased by 44% and 16% (Figures 2E and 2F), respectively, resembling heat-stress phenotypes in Micro-Tom (Figure 1). $lin5^{CR}$ mutants did not show differences from wild type in physiological indices reflecting source activity, including net photosynthetic CO_2 uptake rate (A), internal CO_2 concentration (C_i), and stomatal conductance (g_s) (Figures S1S–S1U), suggesting that source activity does not influence the phenotypes of the mutants. Instead, sucrose accumulation and hexose deficiency occurred in the fruits of $lin5^{CR}$ mutants, reminiscent of the effects caused by heat stress in wild type (Figures 1J–1L and 2G–2I). Together, these results suggest that *LIN5* has major effects on stress-responsive carbon partitioning that accounts for substantial yield loss (Figure 2J).

Integration of a heat-shock element into the *LIN5* promoter confers heat-responsive induction capacity

Because downregulation of *LIN5* underlies yield loss under heat stress, and heat-tolerant tomato varieties often show higher invertase activity,[17] we over-expressed *LIN5* using the ubiquitous *35S* promoter in the Micro-Tom background and found that it did not increase fruit yield (Figure S1V). Instead, the overexpression lines bore phenotypes similar to $lin5^{CR}$ mutant, including reduced height, smaller fruit and leaves (Figures 2K–2M, S1W, and S1X), and decreased yield (Figures 2N, 2O, S1Y, and S1Z). These results, together with source activity unaffected in *LIN5*-overexpression plants (Figures S1S–S1U), suggested that *LIN5* perturbation

Please cite this article in press as: Lou et al., Engineering source-sink relations by prime editing confers heat-stress resilience in tomato and rice, Cell (2025), https://doi.org/10.1016/j.cell.2024.11.005

CellPress

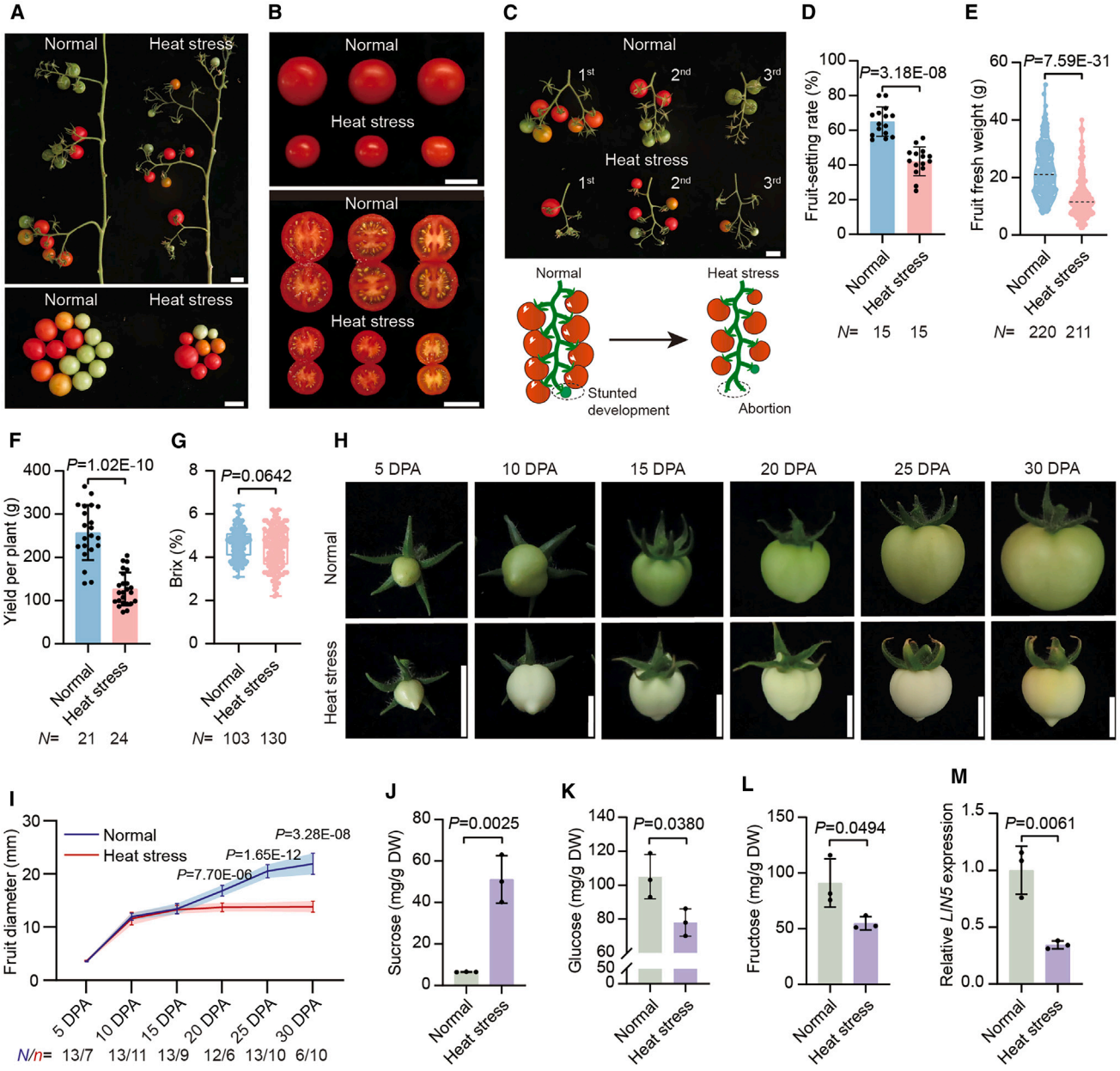

Figure 1. Heat stress disrupts carbon partitioning to fruits by repressing expression of cell-wall invertase *LIN5* in tomato

(A–C) Representative phenotypes of Ailsa Craig shoots (A, upper), total fruit of the first-three trusses (A, lower), fruit transverse sections (B), fruit trusses (C, upper), and fruit abortion (C, lower) under normal conditions or 40°C/30°C day/night heat stress for 14 d in a growth chamber.

(D–G) Quantitative analysis of fruit-setting rate (D), fruit fresh weight (E), yield per plant (F), and sugar content (G) of Ailsa Craig under normal and heat-stress conditions described above.

(H) Representative fruit at different developmental stages under normal (26°C/22°C 16 h day/8 h night) and heat-stress conditions (30°C/26°C 16 h day/8 h night). DPA, days post anthesis.

(I) Fruit growth indicated by comparing fruit diameter between normal conditions and heat-stress conditions at different developmental stages. *N*/*n*, number of individual plants under normal and heat-stress conditions, respectively.

(J–L) Comparison of contents of sucrose (J), glucose (K), and fructose (L) in fruits at 5 DPA between normal and heat-stress conditions in a growth chamber.

(M) Reverse-trascriptase quantitative PCR (RT-qPCR) analysis of *LIN5* expression in fruits at 5 DPA exposed to normal conditions or heat stress (40°C) for 1 h. Data are the mean ± SD, *N* = 3 biological replicates, and relative expression was normalized to *UBIQUITIN*.

N, individual plant number (D and F), fruit number (E and G). Scale bars, 3.5 cm (A and C) and 1 cm (B and H); *p*, two-tailed, two-sample t test (D–G and I–M). Data are mean ± SD (D–G and I–L).

See also Figure S1.

Please cite this article in press as: Lou et al., Engineering source-sink relations by prime editing confers heat-stress resilience in tomato and rice, Cell (2025), https://doi.org/10.1016/j.cell.2024.11.005

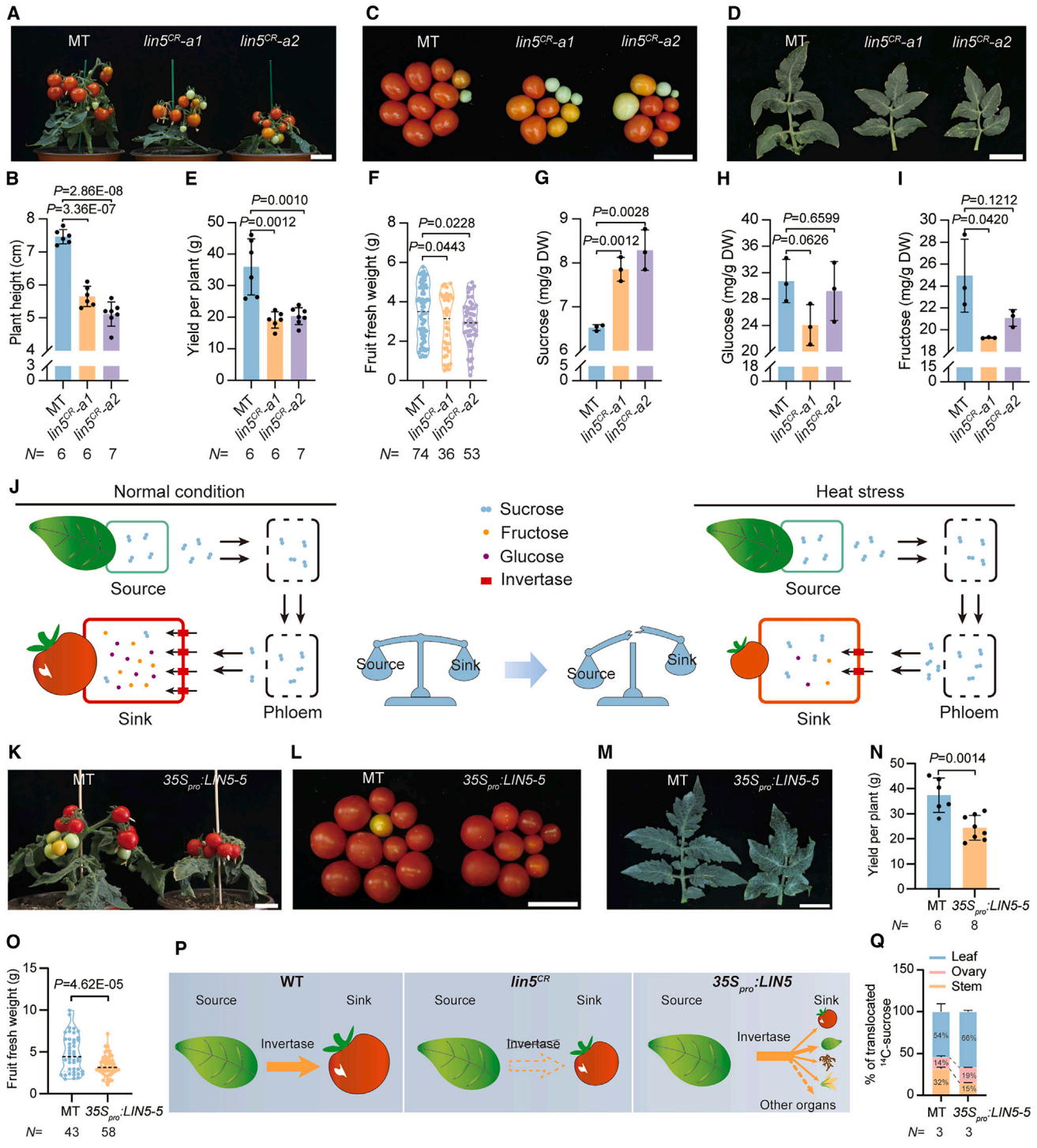

Figure 2. Fine-tuning *LIN5* expression is essential for balancing source-sink relationships

(A–F) Representative phenotypes of wild-type Micro-Tom and *lin5* null alleles *lin5*^{CR}*-a1* and *lin5*^{CR}*-a2* in plant architecture (A), plant height (B), total fruits per plant (C), leaves (D), yield per plant (E), and fruit fresh weight (F).

(G–I) Comparison of contents of sucrose (G), glucose (H), and fructose (I) in fruits at 5 DPA between Micro-Tom and *lin5* null alleles.

(J) Model of invertase-mediated sucrose allocation across apoplasmic interfaces in tomato fruits. Heat stress reduces the abundance of invertases, thereby decreasing the hydrolysis of sucrose into glucose and fructose. This leads to accumulation of sucrose in fruits and inhibits source-to-sink sucrose transport through feedback mechanisms, disrupting the source-sink balance.

(legend continued on next page)

weakens the sink-source balance by disrupting carbon partitioning (Figure 2P). To test this, we performed ^{14}C pulse-chase labeling assay to track source-sink dynamics by feeding the wild-type and *35S$_{pro}$:LIN5-1* plants with ^{14}C-labeled sucrose and monitoring radioactive labeled signals in source and sink organs. Overexpression of *LIN5* leads to over-accumulation of sucrose in leaves, disrupting the source-sink balance (Figure 2Q). Previous reports[22,31] and our findings suggest that fine-tuning *LIN5* expression is instead required to optimize carbon allocation in this context.

Heat-shock elements (HSEs) are recognized by heat-shock transcription factors (HSFs) to rapidly activate gene-expression programs.[39–41] HSFs bind to DNA sequences that have either the nGAAnnTTCn or nTTCnnGAAn HSE motif,[39,42] and the *LIN5* promoter lacks known HSEs. We proposed that targeted integration of an HSE into the *LIN5* promoter might confer heat-responsive regulation to optimize sink activity by fine-tuning *LIN5* expression (Figure 3A). To identify the consensus HSE, we performed a global analysis of promoters of all annotated small heat-shock-protein-targeting genes (*sHSPs*) in *Arabidopsis*, tomato, and rice (Table S1). A palindromic repeat of nGAAnnTTCn or nTTCnnGAAn was enriched (Figures 3B, S2A, and S2B). Among these, the CTAGA motif is frequently observed in stress-responsive genes.[43–45] Considering the effects of sequence length on knockin efficiency and on the chromatin structure of the promoter, we therefore used ATTCTAGAAT as a minimal HSE unit for insertion.

To mitigate disturbances to the endogenous *LIN5* expression pattern owing to HSE insertion, we established basic criteria to select target sites. First, the candidate insertion site should not contain any putatively functional *cis*-element. Second, the insertion site should be located in an open-chromatin region (wherein binding peaks are relatively weak according to publicly available genome-wide databases). Finally, it is preferable for the insertion site to be located within 1 kb of the translational start codon. We scanned 2-kb *LIN5* promoters using PlantCARE to avoid putative *cis*-elements and analyzed chromatin accessibility around the *LIN5* promoter using publicly available DNase-seq and ATAC-seq datasets.[46] A site located 452 bp upstream of the tomato *LIN5* translational start codon was selected as the HSE insertion site (Figure 3C).

We tested whether the chimeric *LIN5* promoter bearing an HSE is functional by dual-luciferase (LUC) reporter assay *in planta* (Figure 3D). *LUC* expression is driven by the native *LIN5* promoter (*LIN5$_{pro}$*), a chimeric *LIN5* promoter with the HSE insertion (*LIN5$_{pro\ +\ HSE}$*), or a scrambled HSE (AGGGTATTTT) (*LIN5$_{pro\ +\ HSE\ scram}$*) serving as a negative control (Figures 3D and 3E). Relative LUC activity from the *LIN5$_{pro\ +\ HSE}$* construct gradually increased after 2 h of heat stress (Figure 3F). By contrast, both *LIN5$_{pro}$* and *LIN5$_{pro\ +\ HSE\ scram}$* did not respond to heat stress, indicating that insertion of HSE endowed the *LIN5* promoter with heat-responsive upregulation capacity. Consistently, the *LIN5$_{pro\ +\ HSE}$* promoter can be specifically recognized and bound by tomato HSFs, in contrast to the *LIN5$_{pro\ +\ HSE\ scram}$* promoter (Figure S2C). Collectively, we have established a pipeline for designing bespoke, stress-responsive chimeric promoters by integrating *in silico* screening with rapid validation *in planta*.

Establishing CROCS by developing a high-efficiency prime-editing system

Transgenic approaches are crucial for crop improvement[47] but are prone to co-suppression and expression attenuation with generation turnover.[48] The heat-responsive property of *LIN5$_{pro\ +\ HSE}$* prompted us to explore the possibility of knocking the HSE into the endogenous *LIN5* promoter by gene editing (Figure 3G). The largest barrier, however, lies in the efficiency and precision of inserting DNA fragments into endogenous genes. Prime editing has been shown to efficiently knock in sequences in animals and monocot plants, but a high-efficiency system is lacking in dicot plants.[49,50] Preventing the prime-editing guide RNA (pegRNA) circularization while maintaining the integrity of the prime-binding site (PBS) and reverse transcriptase (RT) template is essential for pegRNA function and prime-editing efficiency.[51,52] To develop a high-efficiency prime-editing system for dicots, we exploited the 20-nt Csy4 recognition site derived from the type I-F CRISPR-Cas system[53] to inhibit circularization between the PBS and spacer and to prevent pegRNA 3′ degradation by exonucleases (Figures 3G and 3H). We therefore designed a Csy4-based prime-editing system based on the third-generation prime-editing system (PE3), named Csy4-PE (Figure 3H). Specifically, we fused Csy4 protein with the Cas9 (H840A) nickase and RT for expression under the *35S* promoter. The pegRNA and nicking single-guide RNA (nick-sgRNA)—flanked by the Csy4 recognition site—are co-expressed under the *Cestrum* yellow leaf curling virus (*CmYLCV*) promoter.[54] The Csy4 endonuclease binds its recognition site and cleaves fused transcripts to release the pegRNA and nick-sgRNA. The Csy4 recognition site can be retained at the 3′ end of the pegRNA after cleavage to form a hairpin structure to protect its stability (Figure 3G).[51,53]

To examine the editing efficiency, we used the previously published pCXPE01 system as a control (U6-PE)[49] and developed a tRNA-PE system as the second control, where the polycistronic tRNA sequence was fused to both ends of the pegRNA for releasing the guide RNAs without demanding additional promoters.[55] Moreover, we optimized the major prime-

(K–O) Representative phenotypes of shoots (K), total fruits per plant (L), leaves (M), yield per plant (N), and fruit fresh weight (O) of Micro-Tom and the *35S$_{pro}$:LIN5-5* transgenic line.

(P) Model of the source-to-sink relationship in tomato. Loss of *LIN5* results in inefficient carbon supply in fruits and impaired fruit development and final yield. Ectopic *LIN5* overexpression indistinguishably enhances sink strength in leaves, roots, and other organs and disrupts the balance of carbon partitioning, leading to limited fruit development and reduced yield.

(Q) Allocation ratio of ^{14}C-signals in leaves, stems, and ovaries of the wild-type and *35S$_{pro}$:LIN5* plants under normal conditions.

N, individual plant number (B, E, N, and Q), fruit number (F and O). Scale bars, 3.5 cm (A, C, D, K, L, and M); *p*, two-tailed, two-sample t test and data are mean ± SD (B–I, N, O, and Q).

See also Figure S1.

Please cite this article in press as: Lou et al., Engineering source-sink relations by prime editing confers heat-stress resilience in tomato and rice, Cell (2025), https://doi.org/10.1016/j.cell.2024.11.005

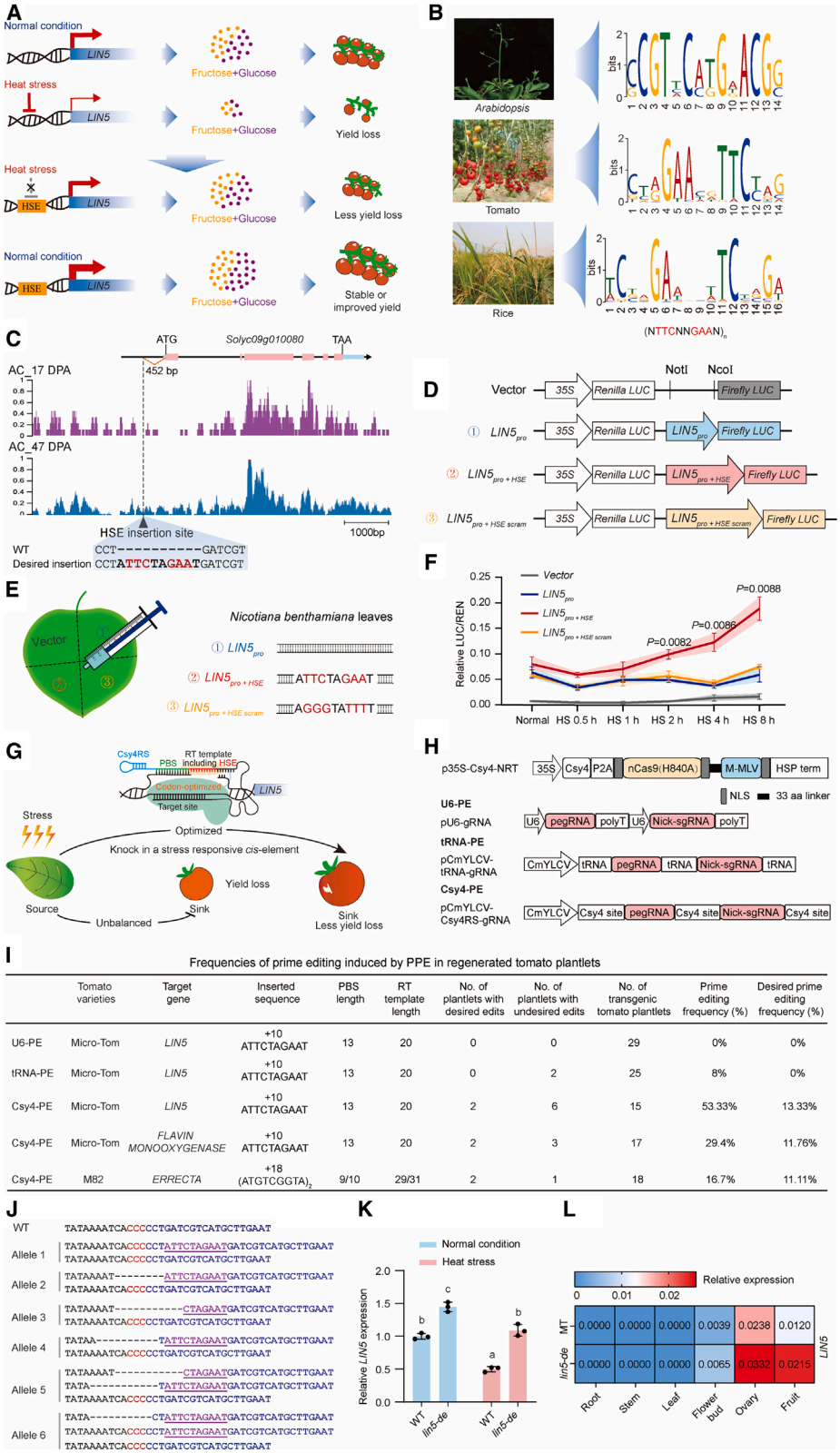

I

Frequencies of prime editing induced by PPE in regenerated tomato plantlets

	Tomato varieties	Target gene	Inserted sequence	PBS length	RT template length	No. of plantlets with desired edits	No. of plantlets with undesired edits	No. of transgenic tomato plantlets	Prime editing frequency (%)	Desired prime editing frequency (%)
U6-PE	Micro-Tom	*LIN5*	+10 ATTCTAGAAT	13	20	0	0	29	0%	0%
tRNA-PE	Micro-Tom	*LIN5*	+10 ATTCTAGAAT	13	20	0	2	25	8%	0%
Csy4-PE	Micro-Tom	*LIN5*	+10 ATTCTAGAAT	13	20	2	6	15	53.33%	13.33%
Csy4-PE	Micro-Tom	*FLAVIN MONOOXYGENASE*	+10 ATTCTAGAAT	13	20	2	3	17	29.4%	11.76%
Csy4-PE	M82	*ERRECTA*	+18 $(ATGTCGGTA)_2$	9/10	29/31	2	1	18	16.7%	11.11%

(legend on next page)

editing components for all above three systems, including the tomato-codon-optimization of RT, the addition of the nuclear-localization sequence at the N terminus of nCas9 and the C terminus of the RT, and insertion of a 33-amino-acid linker between nCas9 and RT (Figure 3H).

To knock in an HSE into the *LIN5* promoter, the Csy4-PE, U6-PE, and tRNA-PE constructs were transformed into Micro-Tom, and independent transgenic lines were recovered (Figure 3I). PCR genotyping and massively parallel sequencing identified various edits, among which two lines (assigned "*lin5-de*" for "desired edit") show precise editing (allele 1) and six lines (assigned "*lin5-ude*" for "undesired edit") with imprecise editing from Csy4-PE system (alleles 2–6, Figures 3I and 3J). Strikingly, our Csy4-PE system reached editing efficiency of 53.3%, with precise editing at 13.3% compared with no editing in U6-PE and no precise editing in tRNA-PE (Figure 3I), representing a high-efficiency prime-editing system for targeted insertion in dicots.[49,50,56–58] Sequencing of PCR amplicons revealed that Csy4-PE exhibited no off-target at all examined sites (Table S2).

To test if the high efficiency of our Csy4-PE system applies to different loci and distinct lengths of insertions in different genetic backgrounds, we first knocked in the same HSE into the promoter of a *FLAVIN MONOOXYGENASE (FMO)* gene (*Solyc09g074430*) that regulates biological processes distinct from *LIN5* (Figure S2D). Desirable editing of *FMO* reached 11.8% (Figures S2E and S2F), comparable to that in *LIN5* (Figure 3I). We then knocked in an 18-bp regulatory sequence into the 5′ UTR of *ERECTA* (*Solyc08g061560*, Figure S2G) using Csy4-PE in a processed tomato variety M82. We achieved a desirable editing rate of 11.1% (Figures S2H and S2I), reproducing the efficiencies observed for *LIN5* and *FMO* (Figure 3I). These results indicate that the Csy4-PE system is an efficient and versatile system for bespoke gene editing in dicot plants.

Knockin of an HSE enhances sink activity and yield in tomato c.v. Micro-Tom

To explore the outcome of the HSE insertion, we first assayed *LIN5* expression in fruits at 5 DPA under normal and heat-stress conditions. *LIN5* was about 1.4-fold higher in *lin5-de* than Micro-Tom under normal conditions and 2.2-fold higher under heat stress (Figure 3K). *LIN5* expression in *lin5-de* under heat stress was comparable to that of Micro-Tom under normal conditions (Figure 3K), suggesting that HSE insertion uncoupled heat-induced repression of *LIN5*. Next, we examined whether the *LIN5* tissue-specific expression pattern was disturbed. Similar to Micro-Tom, *LIN5* was not detected in the roots, stems, and leaves of *lin5-de*, whereas expression in flower buds, ovaries, and fruits was upregulated (Figure 3L), indicating that HSE knockin results in *LIN5* induction specifically in the organs wherein it is normally expressed without ectopic spread.

To assess how fine-tuned *LIN5* expression affects fruit yield, we grew Micro-Tom and *lin5-de* plants under normal conditions in an artificial-climate growth chamber (Figure S3A). *lin5-de* fresh-fruit weight increased by 26% (Figures 4A and 4B), and yield per plant increased by 30% (Figure 4C). Fruit uniformity is an important fruit quality trait that dictates commercial value. Differences in fruit-set timing within the same truss often lead to disuniformity, primarily due to weaker sink activity at the apical end of the truss. Strikingly, unlike wild-type fruits that vary in size, *lin5-de* displayed dramatically improved uniformity (Figure S3B). Moreover, Brix content of *lin5-de* fruits improved by 12% compared with Micro-Tom (Figure 4D). These results indicate that precise knockin of the HSE into *LIN5* improves fruit yield and quality under normal conditions.

Plants were then grown in a growth chamber for a short-term heat-stress treatment (40°C/30°C day/night, Figure 4E). Compared with Micro-Tom, *lin5-de* had 45% and 32% increases in fruit fresh weight and total yield per plant, respectively (Figures 4F and 4G), with a 9% improvement in Brix content (Figure 4H). Heat stress exacerbated fruit disuniformity in Micro-Tom plants but not for *lin5-de* (Figure 4E). To evaluate *lin5-de* performance in a setting mimicking a commercial plastic solar greenhouse typically used to grow table tomatoes, we grew the plants at normal conditions (28°C/19°C day/night) or under a high-temperature regime (33°C/28.5°C day/night, Figures S3C and S3D) for 2 months. Under the normal regime, *lin5-de* had stronger growth vigor than Micro-Tom, manifested by slightly increased plant height and biomass (Figures 4I, S3E, and S3F), implying that enhanced sink activity might promote simultaneous improvement to source-sink relations, as proposed previously.[59,60] Importantly, *lin5-de* increased both fruit fresh weight and total yield per plant by 45% and 46%, respectively (Figures 4J and 4K). Brix content increased by 8% and was accompanied by an improvement in fruit size uniformity in

Figure 3. HSE insertion into the *LIN5* promoter confers a heat-inducible expression property

(A) Schematic of *LIN5* promoter activity and consequences for tomato yield in response to heat stress and its alteration upon knockin of an HSE. Thickness of the red arrows indicates relative *LIN5* expression levels.

(B) Motif analysis of 1-kb promoter regions upstream of heat-shock-protein genes in *Arabidopsis*, tomato, and rice. *N* indicates A/C/G/T; *n* indicates the number of repeats. Red font indicates the core HSE bases.

(C) Identification of DNase-I hypersensitive sites in the *LIN5* promoter from tomato fruits at 17 DPA (top) and 47 DPA (bottom).

(D–F) Schematic constructs (D), experimental design (E), and relative luciferase activity (F) for transient dual-luciferase reporter assay in tobacco. Bases in red font indicate core HSE bases. Data are mean ± SD, $N = 3$ biological replicates (F).

(G and H) Schematics illustrating optimization of source-sink relations by inserting stress-responsive element into the *LIN5* promoter using prime editing (G) and U6-PE, tRNA-PE, and Csy4-PE-based constructs for prime editing in tomato (H).

(I) Frequencies of prime editing induced by U6-PE, tRNA-PE, and Csy4-PE in regenerated tomato plantlets and details of the target sites.

(J) Sequences of different prime-edited *LIN5* alleles derived from Csy4-PE system. Guide RNA and protospacer-adjacent motif (PAM) sequences are highlighted in blue and red; inserted sequences are highlighted in purple and bold underlined, respectively. Black dashes indicate deletions.

(K and L) *LIN5* expression in wild-type and *lin5-de* fruits at 5 DPA under normal and 40°C heat-stress conditions (K) and in different tissues (L). Data are the mean ± SD, $N = 3$ biological replicates, and relative expression was normalized to *UBIQUITIN*. Means with different letters are significantly different ($p < 0.05$, ANOVA). See also Figure S2 and Tables S1 and S2.

Please cite this article in press as: Lou et al., Engineering source-sink relations by prime editing confers heat-stress resilience in tomato and rice, Cell (2025), https://doi.org/10.1016/j.cell.2024.11.005

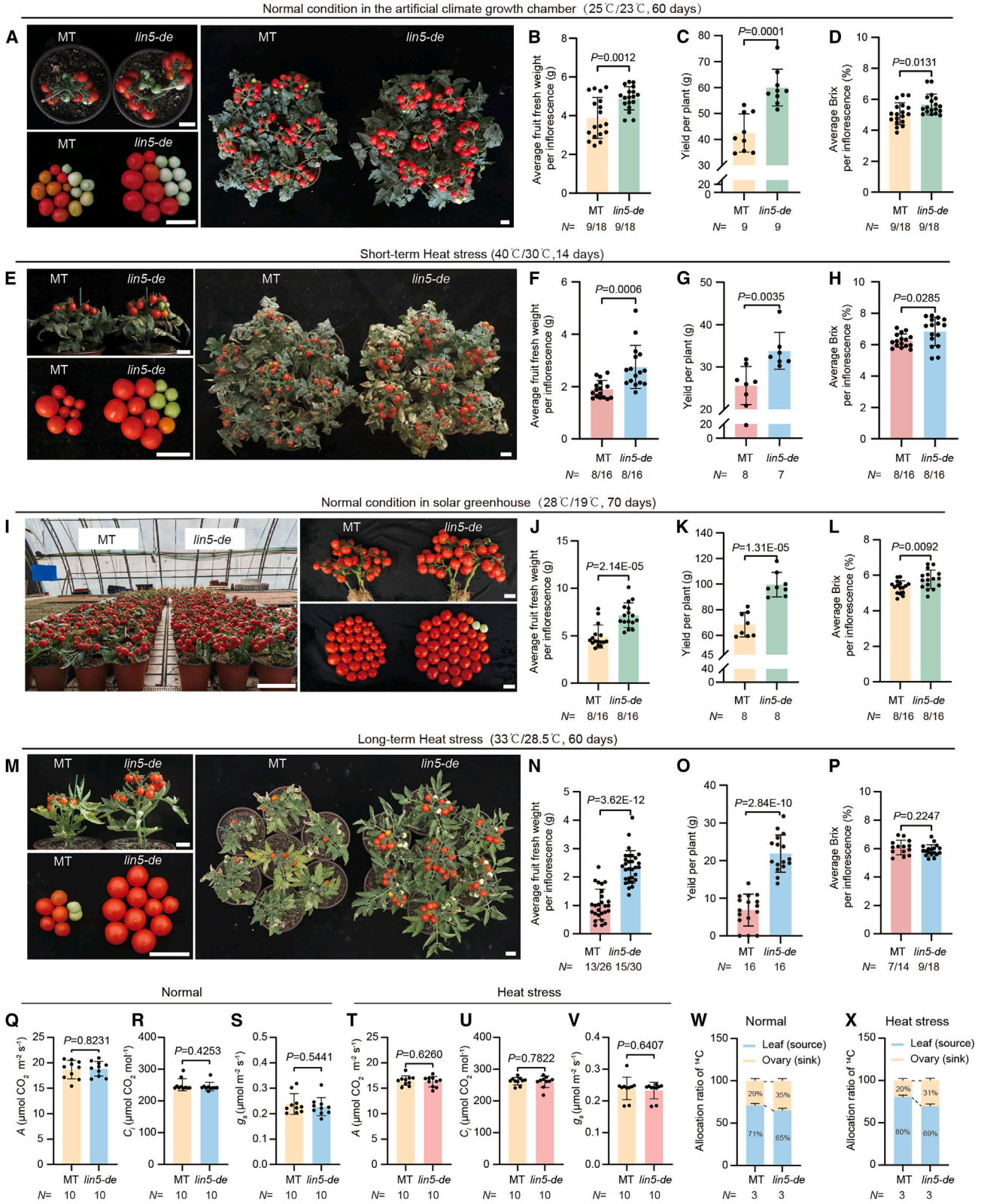

(legend on next page)

Please cite this article in press as: Lou et al., Engineering source-sink relations by prime editing confers heat-stress resilience in tomato and rice, Cell (2025), https://doi.org/10.1016/j.cell.2024.11.005

lin5-de (Figures 4I and 4L). Under the high-temperature regime, Micro-Tom plants had severe fruit abortion and retarded development; however, *lin5-de* plants showed robust growth vigor and produced more fruits (Figure 4M). Fruit fresh weight of *lin5-de* was 128% higher than that of Micro-Tom plants, with greater fruit uniformity (Figures 4M and 4N). Notably, the total fruit yield in *lin5-de* was nearly 4-fold higher than Micro-Tom without differences in fruit Brix content (Figures 4O and 4P).

Improved fruit yield and quality prompted us to investigate source-sink relations in *lin5-de* plants. We measured photosynthesis parameters indicative of source activity[61] but did not find any statistically significant difference between wild-type and *lin5-de* plants under both normal conditions and heat stress (Figures 4Q–4V). We then examined sink activity by ^{14}C pulse-chase assay. Under normal condition, ^{14}C signals in the ovaries of *lin5-de* plants were higher than that in the wild-type (Figure 4W), indicating that *lin5-de* plants have a greater capacity to allocate sucrose to sink organs and thus lead to increased fruit yield under normal condition. Under heat stress, ^{14}C signals over-accumulated in leaves, whereas the proportion of the signal allocated to the ovaries was reduced in wild-type plants (Figures 4W and 4X). However, this heat-induced inhibition of carbon partitioning was markedly alleviated in *lin5-de* plants (Figure 4X), explaining why *lin5-de* plants rescue yield losses under heat stress. Given the frequent occurrence of high temperatures in tomato production, targeted knockin of an HSE into the *LIN5* promoter shows potential for tomato improvement and reducing on-farm losses.

Carbon metabolism and growth genes are differentially expressed in *lin5-de* fruits

To investigate the consequences of HSE insertion into the *LIN5* promoter on source-sink dynamics during fruit development, we performed RNA sequencing (RNA-seq) on fruits at 5 DPA. 1,026 differentially expressed genes were identified (fold change $\geq$ 2, p value < 0.005). Among them, 36.74% (377 genes) were upregulated and 63.25% (649 genes) were downregulated in *lin5-de* (Figure S3G; Table S3). *LIN5* was upregulated approximately 1.3-fold in *lin5-de* fruits under normal conditions (Figures S3H and S3Q). This slight *LIN5* induction also upregulated other regulatory genes involved in source-sink relations (Figure S3I; Table S3). For example, *SlSUT1*, responsible for loading and transporting sucrose from source-to-sink organs,[35] was induced 1.2-fold (Figures S3J and S3R), and *SlSUS*, encoding an enzyme involved in sucrose metabolism,[36] was induced 1.6-fold (Figures S3K and S3S). This indicates that by tweaking *LIN5* expression, genes related to sink strength can be synergistically enhanced. Enhancement of sink activity feeds back to increased source activity,[62] and consistent with this, *SlSPS*, encoding a principal determinant of source strength,[37] was upregulated 1.4-fold in *lin5-de* plants (Figures S3L and S3T). Immature green tomato fruits undergo a period of transient starch accumulation, the conversion of which is important for fruit development. *SlGWD1*, encoding a key enzyme involved in regulating this process,[38] was also upregulated 1.73-fold (Figures S3M and S3U).

Besides genes regulating source-sink dynamics, others involved in reproductive development, especially fruit development and fruit size, were also upregulated due to enhanced sink capacity. For example, *WUSCHEL-RELATED HOMEOBOX 1* (Figures S3N and S3V), known to determine fruit size by promoting shoot-apical-meristem proliferation, carpel, and young fruit development,[63] was 3.2-fold upregulated in *lin5-de* plants. Expression of *fw3.2*, a gene selected during domestication of tomato fruit size and weight,[64] was upregulated 2-fold (Figures S3O and S3W). Final fruit size and weight are regulated by the frequency of cell division and/or the duration of the cell-cycle phase. Accordingly, expression of *CELL-DIVISION PROTEIN KINASE 10* (Figures S3P and S3X), induced by hexose for cell division,[65] was upregulated 3-fold. Together, fine-tuning source-sink genes and fruit-development genes explain the phenotypes of increased fruit fresh weight, improved fruit uniformity, and higher yield for *lin5-de* plants.

CROCS optimizes source-sink relations to rescue heat-induced tomato yield losses in both greenhouse and open field

Improvements in fruit yield and quality from optimized carbon partitioning in Micro-Tom prompted us to investigate utility in the widely used table-tomato variety Ailsa Craig. We transformed the aforementioned prime-editing construct into Ailsa Craig and generated 37 independent transgenic lines. Nine lines were edited, with five desirable edits and a desired-editing efficiency of 13.5% (Figure S4A), validating the high efficiency of our system in tomato.

One line with precise knockin of the HSE, assigned *ac-lin5-de*, was identified and used to produce transgene-free homozygous T_2 progeny to comprehensively score performance in a

Figure 4. Targeted knockin of HSE into the *LIN5* promoter optimizes source-sink carbon partitioning and improves fruit yield in tomato

(A–D) Representative phenotypes of Micro-Tom and *lin5-de* under normal conditions in the artificial-climate growth chamber (A) and related quantification of average fruit fresh weight per inflorescence (B), yield per plant (C), and average Brix per inflorescence (D).

(E–H) Representative phenotypes of growth-chamber-grown Micro-Tom and *lin5-de* plants following short-term heat stress and related quantification of average fruit fresh weight per inflorescence (F), yield per plant (G), and average sugar content per inflorescence (H).

(I–L) Representative phenotypes of Micro-Tom and *lin5-de* plants under normal conditions (28°C/19°C day/night) in a plastic solar greenhouse (I) and related quantification of average fruit fresh weight per inflorescence (J), yield per plant (K), and average sugar content per inflorescence (L).

(M–P) Representative phenotypes of Micro-Tom and *lin5-de* under long-term high-temperature stress (M) and related quantification of average fruit fresh weight per inflorescence (N), yield per plant (O), and average sugar content per inflorescence (P).

(Q–V) Photosynthesis parameters measurement in Micro-Tom and *lin5-de* plants under normal conditions (Q–S) and heat stress (T–V). *N*, individual plant number.

(W and X) Allocation ratio of ^{14}C-signals in leaves (source) and ovaries (sink) of Micro-Tom and *lin5-de* under normal conditions (W) and heat stress (X).

N, number of plants and inflorescences (B, D, F, H, J, L, N, and P), individual plant number (C, G, K, O, W, and X). Scale bars, 3.5 cm (A, E, I, right, and M) and 15 cm (I, left); p, two-tailed, two-sample t test and data are mean ± SD (B–D, F–H, J–L, and N–X).

See also Figure S3 and Table S3.

Please cite this article in press as: Lou et al., Engineering source-sink relations by prime editing confers heat-stress resilience in tomato and rice, Cell (2025), https://doi.org/10.1016/j.cell.2024.11.005

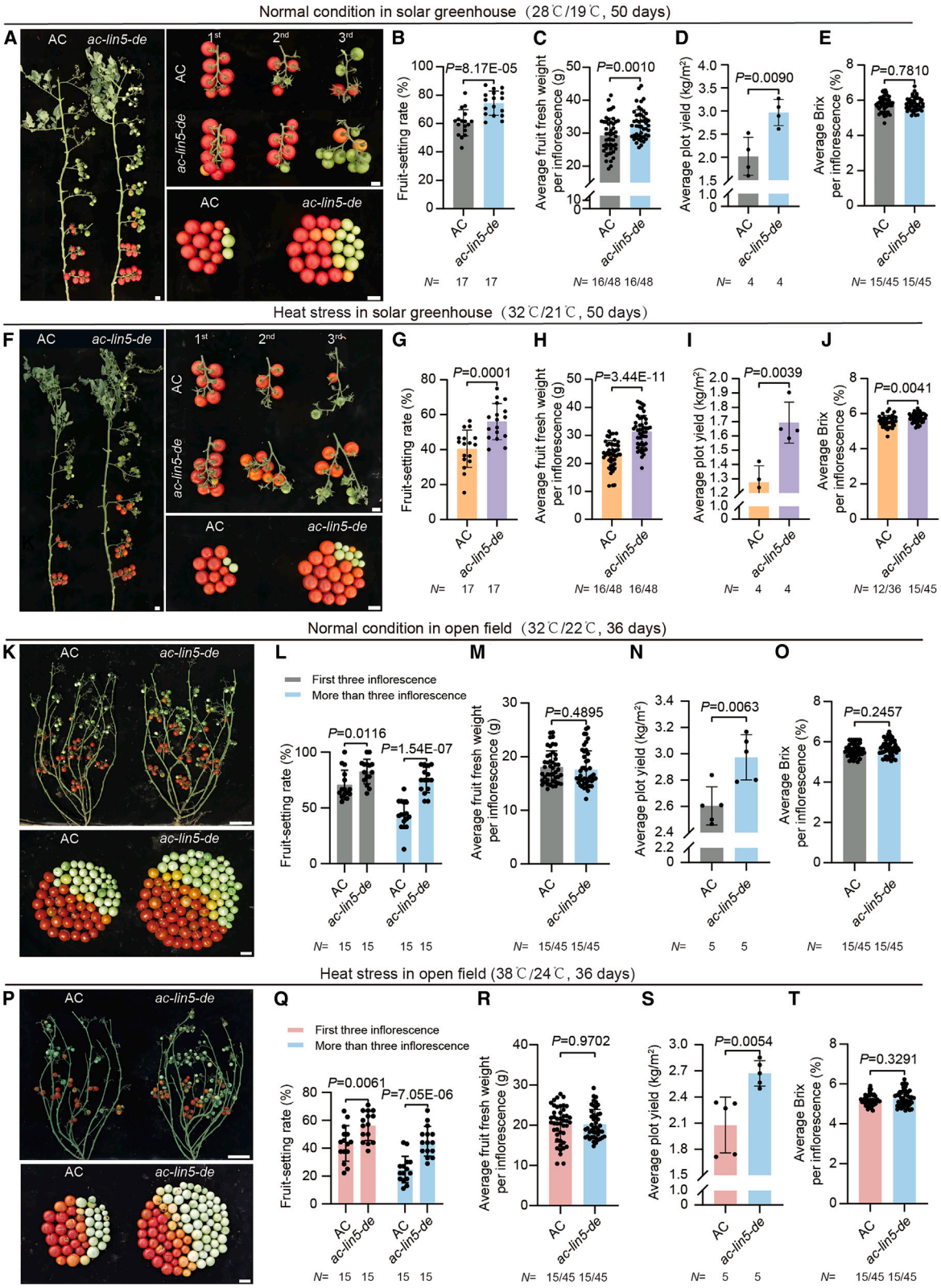

(legend on next page)

commercial plastic solar greenhouse and an open field (Figure 5). Under normal conditions in the greenhouse (28°C/19°C day/night, Figures S4B and S4C), *ac-lin5-de* plants had increased fruit set with an apparent enlargement in fruit size, resulting in an 11% increase in fruit fresh weight compared with Ailsa Craig (Figures 5A–5C). Strikingly, the average plot yield increased by 47% in *ac-lin5-de* without any compromise in Brix content (Figures 5D and 5E).

The indeterminate sympodial growth habit and large biomass of Ailsa Craig make it challenging to conduct large-scale yield trials under heat stress in growth chambers. To overcome this challenge and conduct heat treatments replicating a commercial greenhouse environment, we added an additional layer of transparent plastic film over plants grown in the greenhouse once they started to flower (Figures S4D and S4E). This can lift average daytime temperatures to 32°C (32°C/21°C day/night, Figure S4F) and was sufficient to dramatically reduce fruit set for Ailsa Craig (Figures 5A, 5B, 5F, and 5G), as well as fruit fresh weight (Figures 5C and 5H). Average plot yield was reduced by 36.7% compared with normal conditions (Figures 5D and 5I). Fruit fresh weight and average plot yield were 35% and 33% higher in *ac-lin5-de* plants than that of Ailsa Craig (Figures 5H and 5I). Notably, HSE insertion rescued 56.4% of the yield loss (Figures 5D and 5I), and Brix content also improved in *ac-lin5-de* plants (Figure 5J).

To investigate the performance of HSE-insertion plants across different growth seasons, we conducted a larger scale of plot yield test and treated plants under longer-term higher temperature condition (Figure S4G). *ac-lin5-de* plants showed a 15.7% increase in fresh-fruit weight and an 11.1% increase in fruit-setting rate (Figures S4H and S4I), accompanied by a 7.4% increase in harvest index (Figure S4J), compared with wild-type plants under normal conditions. The average plot fruit yield of *ac-lin5-de* plants increased by 32.8% without compromise in Brix content (Figures S4K and S4L). For the longer-term heat-stress treatment, plants were grown under higher temperatures from seedling stage. The fresh-fruit weight and fruit-setting rate were 8.5% and 21.3% higher in *ac-lin5-de* plants than that of Ailsa Craig controls (Figures S4M and S4N). We investigated the reasons behind increased fruit-settings. Tetrad-stage microspore dissection and pollen staining indicated that HSE insertion did not affect pollen development or viability of mature pollens (Figures S4O–S4T), suggesting that the increased fruit-setting rate in *ac-lin5-de* primarily attributed to improved carbon supply to young fruits, which reduced post-fertilization fruit abortion. Consistently, harvest index and average plot yield of *ac-lin5-de* plants increased by 13.6% and 26.4%, respectively (Figures S4U and S4V) without compromise in Brix content (Figure S4W). These results suggested that targeted knockin of HSE into the *LIN5* promoter increases fruit yield under normal conditions and saves yield losses under heat stress in protected-cultivation mode.

We then surveyed performance of *ac-lin5-de* plants in an open field equipped with real-time temperature sensors in the summer season (Figures S5A and S5B). Under normal conditions in the open field (32°C/22°C day/night), the fruit-setting rate of *ac-lin5-de* plants was significantly higher than Ailsa Craig (Figures 5K and 5L), resulting in an increase of nearly 14% in average plot yield—without penalties for fruit fresh weight and Brix content (Figures 5M–5O). To simulate heat stress in the open field, we covered plants with transparent plastic film once flowering started (Figures S5C and S5D). As expected, heat stress (38°C/24°C day/night) reduced fruit set and yield in both Ailsa Craig and *ac-lin5-de* compared with normal conditions (Figures 5K–5N and 5P–5S). Average plot yield for *ac-lin5-de* was nearly 28% higher than that of Ailsa Craig under heat stress (Figure 5S). Fruit fresh weight and Brix content did not show statistically significant differences (Figures 5R and 5T). Importantly, Ailsa Craig plants lost 20.3% of yield when the average day and night temperature increased by 6°C and 2°C, respectively, but this yield loss was fully rescued in *ac-lin5-de* plants (Figures 5N and 5S), suggesting that knockin of the HSE can achieve stable yields in open field under heat stress.

To test broader applicability of CROCS in different tomato varieties, we performed targeted insertion of HSE into *LIN5* promoters using the same Csy4-PE construct in additional tomato varieties, M82, and a modern fresh tomato inbred line Yuanwei-1 (YW1). Heat-induced repression of *LIN5* occurred in both accessions (Figures S5E and S5F). Expression analysis of *LIN5* in *m82-lin5-de* and *yw1-lin5-de* plants with desirable editing showed similar heat-responsive upregulation observed in Ailsa Craig and Micro-Tom (Figures S5G–S5J). Consistent effects observed across multiple varieties with varying growth habits confirm the reliability and general applicability of the CROCS strategy. Together, HSE targeted insertion achieves thermo-responsive optimization of carbon partitioning by lifting *LIN5* expression under normal conditions, whereas mitigating stress-induced *LIN5* repression under heat stress. CROCS to manipulate *CWIN* expression enables tomato plants to adjust source-sink relations in response to environmental changes, thereby achieving higher yields under normal conditions and

Figure 5. Application of CROCS in tomato cultivar Ailsa Craig enhances fruit yield under normal conditions and saves yield loss under heat stress

(A–E) Representative phenotypes of Ailsa Craig and *ac-lin5-de* grown under normal greenhouse conditions and related quantification of fruit-setting rate (B), average fruit fresh weight per inflorescence (C), average plot yield (D), and average sugar content per inflorescence (E).

(F–J) Representative phenotypes of Ailsa Craig and *ac-lin5-de* grown in greenhouse under mild long-term heat stress (F) and related quantification of fruit-setting rate (G), average fruit fresh weight per inflorescence (H), average plot yield (I), and average sugar content per inflorescence (J).

(K–T) Representative phenotypes of shoots and total fruits per plant of Ailsa Craig and *ac-lin5-de* grown in the open field under normal (K) and high-temperature conditions (P) and related quantification of fruit-setting rate (L and Q), average fruit fresh weight per inflorescence (M and R), average plot yield (N and S), and average sugar content per inflorescence (O and T).

N, number of plants and inflorescences (C, E, H, J, M, O, R, and T), individual plant number (B, G, L, and Q), and yield plot number (D, I, N, and S). Scale bars, 3.5 cm (A, F, K, and P); *p*, two-tailed, two-sample t test and data are mean ± SD (B–E, G–J, L–O, and Q–T).

See also Figures S4 and S5.

Please cite this article in press as: Lou et al., Engineering source-sink relations by prime editing confers heat-stress resilience in tomato and rice, Cell (2025), https://doi.org/10.1016/j.cell.2024.11.005

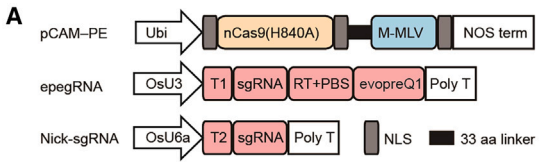

B

Frequencies of prime editing induced by PPE in regenerated rice plantlets

Desired edit type	PBS length	RT template length	No. of plantlets with desired edits	No. of plantlets with undesired edits	No. of transgenic tomato plantlets	Prime editing frequency (%)
+10 ATTCTAGAAT	13	20	3	0	37	8.1%

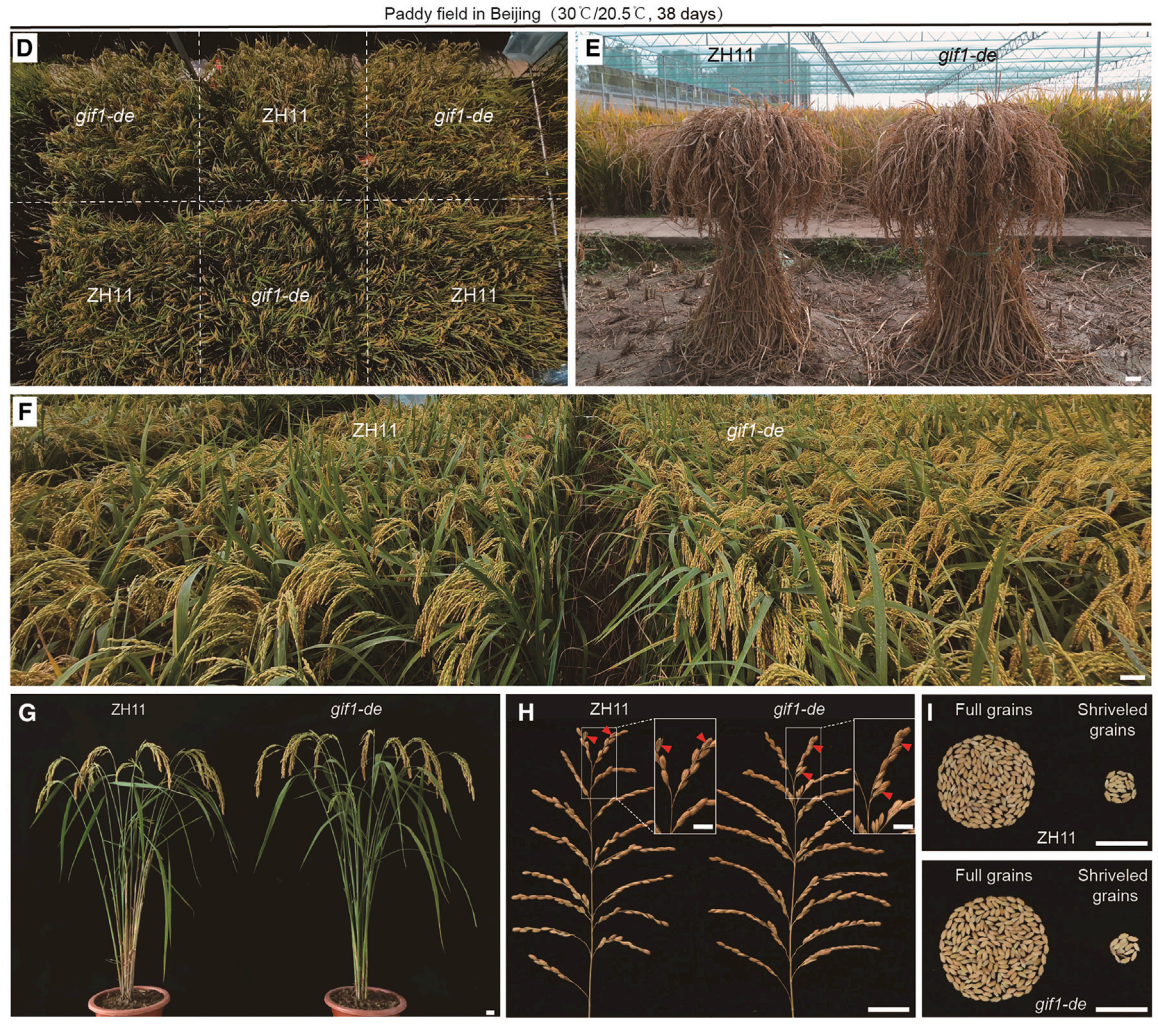

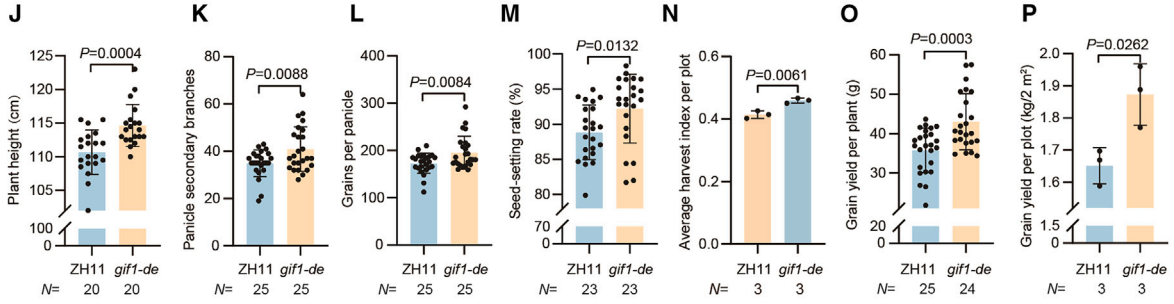

(legend on next page)

stable yields under heat stress in different cultivation settings (Figure 3A).

CROCS delivers efficient prime editing in rice and lifts yield in paddy fields

Given the conservation of cell-wall-invertase function in plants and successfully engineering *LIN5* functions in various tomato varieties, we next sought to deploy CROCS by targeting cell-wall-invertase in a staple cereal. Mutations in the *GIF1* promoter were selected during rice domestication[20,66] but were not further selected in breeding elite modern rice germplams.[67] We therefore exploited the crop improvement potential of cell-wall-invertase engineering in rice by inserting HSE into the *GIF1* promoter. We adapted our tomato-optimized prime-editing system for rice. We based it on the pCAMBIA1300 vector[68] by introducing a rice-codon-optimized M-MLV RT and a novel structural RNA motif, evopreQ1[52] at the 3′ end of the pegRNA to protect it from exonuclease degradation and named it pCAM-PE (Figure 6A). By following the aforementioned three criteria for target-site selection, we selected the −427-bp position to insert the HSE. We chose a *japonica* rice cultivar Zhonghua 11 (ZH11), an experimental staple of rice genetics and biotechnology, as the target variety.[69] Thirty-seven independent transgenic lines were obtained, of which three lines (*gif1-de*) bear precise insertions of the HSE. Precise desirable editing efficiency reached 8.1% (Figures 6B and 6C). Sequencing of PCR amplicons of three top-scoring off-target sites excluded the off-targeting effects (Table S2).

We evaluated the performance of transgene-free homozygous *gif1-de* plants in paddy fields equipped with real-time temperature sensors at Beijing and Hainan in plots with densities typically used by local farmers (Figures 6D, S6A, and S6B). Under normal conditions (30°C/20.5°C day/night at heading stage) in Beijing, *gif1-de* plants in each plot generally exhibited increased growth vigor, better uniformity, and fuller panicles compared with ZH11 (Figures 6D–6F). These plants had no significant differences from ZH11 in tiller number, panicle length, number of primary panicle branches, and 1,000-grain weight (Figures 6G–6I and S6C–S6F). However, they showed marked increases in plant height, number of secondary panicle branches, and the number of grains per panicle (Figures 6G–6L). These phenotypes indicate that HSE insertion into the *GIF1* promoter is likely to optimize source-sink relations by enhancing carbon partitioning, similar to tomatoes. Supporting this, *gif1-de* had a 7% increase in seed-setting rate and a 10.8% increase in harvest index with fewer shriveled or empty grains compared with ZH11 (Figures 6I, 6M, and 6N). Grain yield per plant and grain yield per plot increased by approximately 20% and 13% in *gif-de* plants, respectively (Figures 6O and 6P).

We conducted a larger-scale yield trial in Hainan, a different climatic region from Beijing. 13,260 rice plants per genotype were planted in five blocks, with each block composed of two plots covering an area of 100 m^2 and containing 2,652 plants (Figures 7A and 7B). Under normal conditions (29°C/20°C day/night at heading stage) (Figures 7A and S6G), *gif1-de* plants did not show significant differences from ZH11 in tiller number, plant height, panicle length, the number of primary panicle branches (Figures S6H–S6M), and 1,000-grain weight (Figures 7F and S6I). However, *gif1-de* plants showed increases in the number of secondary panicle branches (Figure 7C), seed-setting rate (Figure 7D), and number of grains per panicle (Figure 7E), consistent with phenotypes observed in Beijing (Figures 6K–6M). Accordingly, grain yield per plant and grain yield per block increased by approximately 8.5% and 7.5% in *gif-de* plants, respectively (Figures 7G and 7H). These results demonstrate that knockin of the HSE into the *GIF1* promoter improves sink-organ growth and increases grain yields in rice under normal conditions.

Bespoke prime editing of *GIF1* rescues heat-induced yield losses in rice

Heat stress at the grain-filling stage inhibits the conversion of sucrose into hexoses and thus causes abortion and empty grains.[20,33] Every 1°C increase in minimum seasonal growing temperature can cause grain yield by about 10% in rice.[33] To test if the CROCS strategy applies to rice in saving yield losses under heat stress, we grew ZH11 and *gif-de* plants in the paddy field covered with transparent plastic film as previously reported[70] (Figures 7I–7K and S6A). Temperatures increased by approximately 5°C in the daytime and by 3°C at night (36°C/24°C day/night at heading stage) (Figure S6N). This heat-stress condition reduced plant height and tiller number for ZH11 (Figures S6O and S6P). Although panicle length and branch numbers were unchanged, the seed-setting rate and number of grains per panicle decreased by 16.3% and 18.9% (Figures S6Q and S6R), and 1,000-grain weight decreased by 7.4% under heat stress (Figure S6S), resulting in yield-per-plant and yield-per-plot losses of 32.2% and 37.9%, respectively

Figure 6. Knockin of HSE into the promoter of *GIF1* in rice optimizes source-sink relations and improves grain yield

(A) Schematics of the pCAM-PE system for HSE insertion in rice.

(B) Frequencies of prime editing in regenerated rice plantlets and details of the target sites.

(C) Sequences of *gif1-de* edited alleles in ZH11 background. Guide RNA and PAM sequences are highlighted in blue and red; the inserted sequence is highlighted in purple and bold underlined, respectively.

(D and E) Top review of rice plants grown in yield plots (D) and harvested plants of ZH11 and *gif1-de* grown in each plot (E) in the paddy field in Beijing, China. The white dashed lines separate each plot.

(F–I) Representative images showing panicles with filled grains for populations in the field (F), plant architecture (G), panicles (H), and total grains per panicle (I) of ZH11 and *gif1-de* under normal conditions grown in the field. Red arrows indicate empty and aborted grains.

(J–P) Quantification of plant height (J), number of secondary branches per panicle (K), number of grains per panicle (L), seed-setting rate (M), harvest index (N), grain yield per plant (O), and grain yield per plot (P) of ZH11 and *gif1-de* under normal conditions grown in the field.

N, individual plant number (J, M, and O), panicle number (K and L), and yield plot number (N and P). *p*, two-tailed, two-sample t test and data are mean ± SD (J–P). Scale bars, 10 cm (E and F), 3.5 cm (G–I), and 1 cm (insets in H).

See also Figures S6 and S7 and Table S2.

Please cite this article in press as: Lou et al., Engineering source-sink relations by prime editing confers heat-stress resilience in tomato and rice, Cell (2025), https://doi.org/10.1016/j.cell.2024.11.005

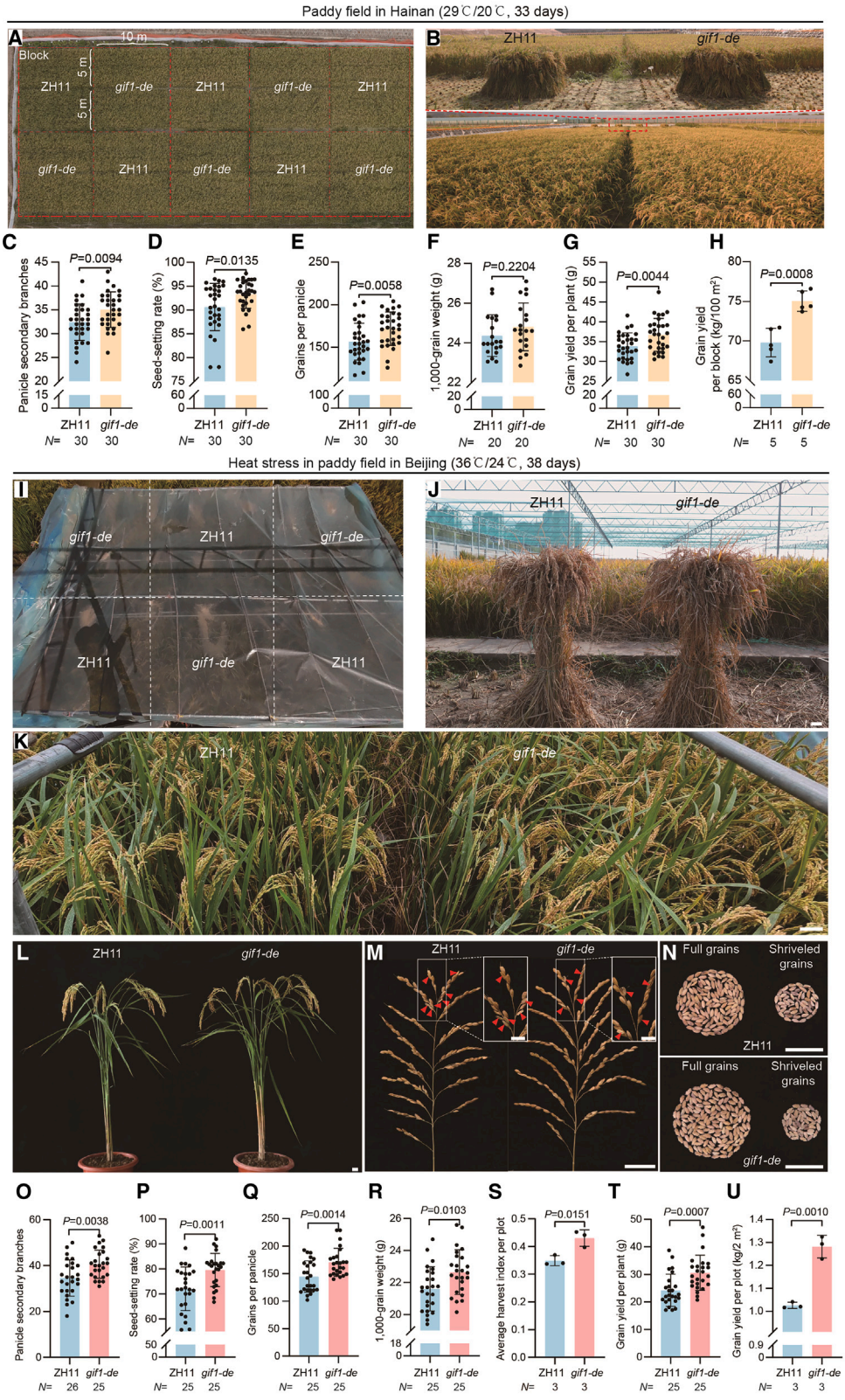

(legend on next page)

(Figures S6T and S6U). These results indicated that heat stress causes substantial yield loss due to reproductive development failure of sink organs in rice.

We then compared ZH11 and *gif1-de* source-sink relations and growth performance under heat stress. No statistically significant changes were observed for tiller number, plant height, panicle length, and number of primary panicle branches between *gif1-de* and ZH11 (Figures 7L, 7M, and S6V–S6Y). However, the number of secondary panicle branches increased by 7% in *gif1-de* (Figures 7M and 7O). Secondary and higher-order branches preferentially incur floral and seed abortion compared with primary parts of panicles due to inefficient carbon partitioning under stress condition.[71,72] Seed-setting rate for *gif1-de* plants increased by 10.5% (Figure 7P) with an 11.8% increase in the last-three high-order panicle branches (Figure S6Z), leading to more grains per panicle (Figures 7N and 7Q). These results suggested that knockin of HSE into the *GIF1* promoter simultaneously promotes high-order panicle branches and mitigates seed abortions. These improvements were also accompanied by a 4.9% increase in 1,000-grain weight and a 23.3% increase in harvest index in *gif1-de* (Figures 7R and 7S), indicating coordinated optimization of sink activity for reproductive development. Such improvements in sink-organ growth resulted in a 26% increase in grain yield per plant and a 25% increase in grain yield per plot in *gif1-de* compared with ZH11 (Figures 7T and 7U). Notably, the *gif1-de* plants rescued 40.9% of the yield loss caused by heat stress (Figures 6P and 7U).

To assess whether CROCS applies to more elite modern rice germplasms, we first surveyed if *GIF1* has been deployed during breeding selection. An integrated genomic analysis using a large permanent population of 18,421 rice lines revealed that *GIF1* is not a causal gene for yield traits.[67] We then exploited pan-genome data from diverse rice accessions to compare ZH11 with 16 elite modern germplasms (Table S4). They showed high *GIF1* sequence similarity to ZH11, with no notable haplotype disparities (Figure S7A). Further analysis of the HSE insertion region in the *GIF1* promoter also displayed high sequence consensus between ZH11 and elite modern varieties (Figure S7A), suggesting a similar improvement potential for targeted HSE insertion into this region in additional elite varieties.

To validate this, we selected three recently approved and widely planted elite varieties from aforementioned elite accessions, namely, Wuyoudao-4 (WYD-4), Longgeng-31, and Zhongkefa-5, to analyze *GIF1* expression. Heat stress repressed *GIF1* expression in all three varieties, and the extent of heat repression is indistinguishable from ZH11 (Figures S7B–S7E), consistent with the genome-wide analysis that *GIF1* has not been improved in these varieties. We used the same prime-editing construct utilized for ZH11 to knock in the HSE into the WYD-4 *GIF1* promoter. T_0 plants with desirable HSE insertion (*wyd-4-gif1-de*) were obtained for analyzing *GIF1* expression, using non-edited WYD-4 T_0 plants as the wild-type control. Under normal conditions, *GIF1* was upregulated in *wyd-4-gif1-de* (Figure S7F). Under heat stress, HSE insertion alleviated *GIF1* repression and enhanced it expression by 1.96 times compared with controls, resembling effects observed in *gif1-de* and ZH11 plants (Figures S7G–S7I). Five independent T_0 plants of *wyd-gif1-de* and non-edited WYD-4 were used for a preliminary phenotypic comparison. The *wyd-gif1-de* plants showed larger grain size with a 10.4% increase of 1,000-grain weight (Figures S7J and S7K). Accordingly, grain yield per plant and harvest index increased by approximately 23.3% and 7.8% in *wyd-gif1-de* plants, respectively (Figures S7L and S7M). These results suggest that rational design of *GIF1* expression by CROCS offers an efficient approach to unlocking its potential in crop improvement, which complements traditional breeding methods and creates valuable genetic variation that may have been overlooked or underexplored in conventional breeding practices.

DISCUSSION

Since the proposal of source-sink theory in 1928,[12] it has played a crucial role in fundamental plant physiology and developmental biology[9,13,28,73] and extends to agricultural production and food security.[14,60,74] With a deepened understanding of its regulatory mechanisms and the rise of genetic-engineering techniques, such as transgenics or gene editing to knock genes out, source-sink-related genes have been manipulated to certain extents.[20,38,75–77] However, this is often accompanied by a trade-off that imbalances carbon partitioning and results in penalties.[31,66] Furthermore, many source-sink-related genes require only moderate upregulation to exert their functions,[76] but high-efficiency tools to achieve such expression levels are still lacking. As modern crop breeding becomes more intensive and integrative genomics methods advance, most important yield genes have been identified and used,[67] highlighting the urgent need to

Figure 7. Application of CROCS in the elite *japonica* rice cultivar improves grain yield under normal conditions and rescues yield losses under heat stress

(A) Top view of plants grown in yield plots in the paddy field in Hainan, China. The red dashed lines separate each block (every two plots).

(B) Representative images of all harvested plants per plot (upper) and the population after grain filling in the paddy field (lower). All plants grown in each plot were harvested, and red dashed lines indicate two plots selected for imaging.

(C–H) Quantification of panicle secondary branches (C), seed-setting rate (D), grains per panicle (E), 1,000-grain weight (F), grain yield per plant (G), and grain yield per block (H) in ZH11 and *gif1-de* under normal conditions in the field as described in (A).

(I) Top view of plots covered with plastic film for heat-stress treatment in the paddy field in Beijing, China. The white dashed lines separate each plot.

(J–N) Representative images showing harvested rice plants per plot (J), panicles with filled grains for populations in the field (K), plant architecture (L), panicles (M), and total grains per panicle (N) of ZH11 and *gif1-de* under heat stress in the field. Red arrows indicate empty and aborted grains.

(O–U) Quantification of panicle secondary branches (O), seed-setting rate (P), grains per panicle (Q), 1,000-grain weight (R), harvest index (S), grain yield per plant (T), and grain yield per plot (U) of ZH11 and *gif1-de* under heat stress in the field.

N, individual plant number (D, F, G, P, R, and T), panicle number (C, E, O, and Q), yield plot number (S and U), and yield block number (H). Scale bars, 10 cm (J and K), 3.5 cm (L–N), and 1 cm (insets in M); *p*, two-tailed, two-sample t test and data are mean ± SD (C–H and O–U).

See also Figures S6 and S7.

Please cite this article in press as: Lou et al., Engineering source-sink relations by prime editing confers heat-stress resilience in tomato and rice, Cell (2025), https://doi.org/10.1016/j.cell.2024.11.005

enrich genetic pool to increase yield to face global climate change and population growth. If new approaches can endow source-sink-related genes with the ability to self-regulate in response to environmental changes, it could create new genetic variation and achieve high yields under favorable conditions, as well as stable yields under adverse conditions.

In this study, we have developed the CROCS strategy by establishing a high-efficiency prime-editing system that allows the precise insertion of heat-responsive elements into the promoter of an important carbon partitioning gene *CWIN*. This bespoke editing endowed elite tomato and rice varieties with a refined response to heat stress by upregulating *LIN5/GIF1* expression without disrupting its spatial expression pattern. Such expression tips the balance of carbon partitioning on the heat-stress response back toward growth and development to consequently improve yield in two major crops under commercial-cultivation settings and save yield losses from heat stress. This strategy rapidly and precisely realizes the optimization of source-sink relations and confers a major step toward the long-term goal of higher yield under favorable conditions and stable yield under adverse conditions.

Extensive research has identified numerous central-hub genes related to yield, quality, and stress tolerance across different crops. Unfortunately, many of these genes connect to multiple gene networks and come with a "more is not better" effect when ectopically expressed or are knocked out, leading to yield penalties or fitness costs.[69,78–80] Rational design of their regulatory regions using gene editing to achieve bespoke, climate-smart expression patterns could allow for the rapid deployment of such genes in breeding, thereby enriching the breeding gene pool and dramatically improving breeding efficiency. Fortunately, many *cis*-regulatory elements have been identified to respond to various stresses.[81] CROCS offers an efficient and precise breeding strategy for rapidly creating climate-smart crops to meet future food demands. Moreover, it also provides versatile tools and feasible approaches for fundamental discovery work that pave the way, in turn, for delivery. More broadly, the introduction of climate-responsive *cis*-elements will drive the direct evolution of regulatory sequences in plant genes, endowing genes with new spatiotemporal expression patterns. This, in turn, rewires the molecular networks of gene expression in response to environmental changes, providing new insights for studying the molecular relationships between genotype, phenotype, and environment as well as their adaptation to ecosystems.

Limitations of the study

Despite efficiently and precisely inserting an HSE into different gene promoters from different species using our optimized prime-editing systems and proposing principles for the selection of target sites, the complexity of chromatin structure itself means that there is still a degree of uncertainty in target selection, and it cannot be guaranteed that all selected targets can achieve efficient and precise insertion. This scenario is similar to the situation when designing target sites for CRISPR-Cas9 gene editing. Despite some targets scoring high in all design criteria, certain targets may still be uneditable due to the complexity of chromatin structure or other unknown reasons. This necessitates changes to other targets based on principles around target selection. Moreover, most current tomato and rice varieties are hybrids, and their parental lines are proprietary to seed companies and inaccessible to most academic labs. We therefore used multiple different available modern elite tomato and rice varieties for engineering and conducted yield trials under different cultivation modes, planting scales, climate regions, field locations, and growing seasons.

RESOURCE AVAILABILITY

Lead contact

Further information and requests for resources and reagents should be directed to and will be fulfilled by the lead contact, Cao Xu (caoxu@genetics.ac.cn).

Materials availability

All unique/stable reagents generated in this study are available from the lead contact with a completed materials transfer agreement.

Data and code availability

The RNA-seq data have been deposited in the Genome Sequence Archive (GSA; https://ngdc.cncb.ac.cn/gsa/) at the Beijing Institute of Genomics (BIG) Data Center, Chinese Academy of Sciences, under accession number PRJCA024921. The accession number was listed in the key resources table. Any additional information required to reanalyze the data reported in this work paper is available from the lead contact upon request.

ACKNOWLEDGMENTS

We thank Prof. Jiayang Li, Prof. Guifu Liu, and Dr. Mingjiang Chen for kindly providing rice varieties, including Wuyoudao-4, Longgeng-31, and Zhongkefa-5. We thank Prof. Xuehui Huang, Prof. Zuhua He, and Dr. Yanhui Jing for discussions and valuable comments. We thank Dr. Hongjie Zhang and Dr. Jinye Mou for assisting us with the detection of radioactivity. We thank Yaoyao Wang and Qilin Yang for assistance in sucrose and hexose measurements. We thank Dr. Bo Ming, Anbang Lin, Xun Yu, and Tiantian Jiang for helping with paddy field imaging. We thank members of the Xu laboratory, especially Xuchen Yu, Yezi Lu, Ling Ye, and Liang He, for assistance with data collection and analysis. This research was supported by the National Natural Science Foundation of China (32225045, 32388101, and 31991183 to C.X.) and the Strategic Priority Research Program of Chinese Academy of Sciences (grant no. XDA24030503 and XDB1090301 to C.X. and XDB1090202 to S.L.).

AUTHOR CONTRIBUTIONS

C.X. designed and supervised the research. H.L., S.L., Z.S., Y. Zou, Y. Zhang, X.H., D.Y., Y.Y., and Z.L. performed the experiments. H.L. and S.L. analyzed the data and prepared figures. C.X. wrote the paper with input from H.L. and S.L.

DECLARATION OF INTERESTS

The authors are named inventors on a number of patents and patent applications directly related to this technology.

STAR★METHODS

Detailed methods are provided in the online version of this paper and include the following:

- KEY RESOURCES TABLE
  - Experimental model and study participant details
- METHOD DETAILS
  - Heat-stress experiments and data collection

SUPPLEMENTAL INFORMATION

Supplemental information can be found online at https://doi.org/10.1016/j.cell.2024.11.005.

Received: April 2, 2024
Revised: September 26, 2024
Accepted: November 7, 2024
Published: December 13, 2024

REFERENCES

1. van Dijk, M., Morley, T., Rau, M.L., and Saghai, Y. (2021). A meta-analysis of projected global food demand and population at risk of hunger for the period 2010–2050. Nat. Food *2*, 494–501. https://doi.org/10.1038/s43016-021-00322-9.
2. Wheeler, T., and von Braun, J. (2013). Climate change impacts on global food security. Science *341*, 508–513. https://doi.org/10.1126/science.1239402.
3. Ray, D.K., Sloat, L.L., Garcia, A.S., Davis, K.F., Ali, T., and Xie, W. (2022). Crop harvests for direct food use insufficient to meet the UN's food security goal. Nat. Food *3*, 367–374. https://doi.org/10.1038/s43016-022-00504-z.
4. Zhao, C., Liu, B., Piao, S., Wang, X., Lobell, D.B., Huang, Y., Huang, M., Yao, Y., Bassu, S., Ciais, P., et al. (2017). Temperature increase reduces global yields of major crops in four independent estimates. Proc. Natl. Acad. Sci. USA *114*, 9326–9331. https://doi.org/10.1073/pnas.1701762114.
5. Wang, X., Zhao, C., Müller, C., Wang, C., Ciais, P., Janssens, I., Peñuelas, J., Asseng, S., Li, T., Elliott, J., et al. (2020). Emergent constraint on crop yield response to warmer temperature from field experiments. Nat. Sustain. *3*, 908–916. https://doi.org/10.1038/s41893-020-0569-7.
6. Hickey, L.T., N Hafeez, A., Robinson, H., Jackson, S.A., Leal-Bertioli, S.C.M., Tester, M., Gao, C., Godwin, I.D., Hayes, B.J., and Wulff, B.B.H. (2019). Breeding crops to feed 10 billion. Nat. Biotechnol. *37*, 744–754. https://doi.org/10.1038/s41587-019-0152-9.
7. Reynolds, M., Atkin, O.K., Bennett, M., Cooper, M., Dodd, I.C., Foulkes, M.J., Frohberg, C., Hammer, G., Henderson, I.R., Huang, B., et al. (2021). Addressing research bottlenecks to crop productivity. Trends Plant Sci. *26*, 607–630. https://doi.org/10.1016/j.tplants.2021.03.011.
8. Mohd Saad, N.S., Neik, T.X., Thomas, W.J.W., Amas, J.C., Cantila, A.Y., Craig, R.J., Edwards, D., and Batley, J. (2022). Advancing designer crops for climate resilience through an integrated genomics approach. Curr. Opin. Plant Biol. *67*, 102220. https://doi.org/10.1016/j.pbi.2022.102220.
9. Fernie, A.R., Bachem, C.W.B., Helariutta, Y., Neuhaus, H.E., Prat, S., Ruan, Y.L., Stitt, M., Sweetlove, L.J., Tegeder, M., Wahl, V., et al. (2020). Synchronization of developmental, molecular and metabolic aspects of source-sink interactions. Nat. Plants *6*, 55–66. https://doi.org/10.1038/s41477-020-0590-x.
10. Shen, S., Ma, S., Wu, L., Zhou, S.L., and Ruan, Y.L. (2023). Winners take all: competition for carbon resource determines grain fate. Trends Plant Sci. *28*, 893–901. https://doi.org/10.1016/j.tplants.2023.03.015.
11. Ruan, Y.L. (2014). Sucrose metabolism: gateway to diverse carbon use and sugar signaling. Annu. Rev. Plant Biol. *65*, 33–67. https://doi.org/10.1146/annurev-arplant-050213-040251.
12. Mason, T.G., and Maskell, E.J. (1928). Studies on the transport of carbohydrates in the cotton plant: II. the factors determining the rate and the direction of movement of sugars1. Annals of Botany *os–42*, 571–636. https://doi.org/10.1093/oxfordjournals.aob.a090131.
13. Ruan, Y.L., Jin, Y., Yang, Y.J., Li, G.J., and Boyer, J.S. (2010). Sugar input, metabolism, and signaling mediated by invertase: roles in development, yield potential, and response to drought and heat. Mol. Plant *3*, 942–955. https://doi.org/10.1093/mp/ssq044.
14. Aluko, O.O., Li, C., Wang, Q., and Liu, H. (2021). Sucrose utilization for improved crop yields: a review article. Int. J. Mol. Sci. *22*, 4704. https://doi.org/10.3390/ijms22094704.
15. Sturm, A., and Tang, G.Q. (1999). The sucrose-cleaving enzymes of plants are crucial for development, growth and carbon partitioning. Trends Plant Sci. *4*, 401–407. https://doi.org/10.1016/s1360-1385(99)01470-3.
16. Wang, L., Li, X.R., Lian, H., Ni, D.A., He, Y.K., Chen, X.Y., and Ruan, Y.L. (2010). Evidence that high activity of vacuolar invertase is required for cotton fiber and *Arabidopsis* root elongation through osmotic dependent and independent pathways, respectively. Plant Physiol. *154*, 744–756. https://doi.org/10.1104/pp.110.162487.
17. Li, Z., Palmer, W.M., Martin, A.P., Wang, R., Rainsford, F., Jin, Y., Patrick, J.W., Yang, Y., and Ruan, Y.L. (2012). High invertase activity in tomato reproductive organs correlates with enhanced sucrose import into, and heat tolerance of, young fruit. J. Exp. Bot. *63*, 1155–1166. https://doi.org/10.1093/jxb/err329.
18. Tieman, D., Zhu, G., Resende, M.F.R., Jr., Lin, T., Nguyen, C., Bies, D., Rambla, J.L., Beltran, K.S.O., Taylor, M., Zhang, B., et al. (2017). A chemical genetic roadmap to improved tomato flavor. Science *355*, 391–394. https://doi.org/10.1126/science.aal1556.
19. Gao, L., Gonda, I., Sun, H., Ma, Q., Bao, K., Tieman, D.M., Burzynski-Chang, E.A., Fish, T.L., Stromberg, K.A., Sacks, G.L., et al. (2019). The tomato pan-genome uncovers new genes and a rare allele regulating fruit flavor. Nat. Genet. *51*, 1044–1051. https://doi.org/10.1038/s41588-019-0410-2.
20. Wang, E., Wang, J., Zhu, X., Hao, W., Wang, L., Li, Q., Zhang, L., He, W., Lu, B., Lin, H., et al. (2008). Control of rice grain-filling and yield by a gene with a potential signature of domestication. Nat. Genet. *40*, 1370–1374. https://doi.org/10.1038/ng.220.
21. Fridman, E., Carrari, F., Liu, Y.S., Fernie, A.R., and Zamir, D. (2004). Zooming in on a quantitative trait for tomato yield using interspecific introgressions. Science *305*, 1786–1789. https://doi.org/10.1126/science.1101666.
22. Zanor, M.I., Osorio, S., Nunes-Nesi, A., Carrari, F., Lohse, M., Usadel, B., Kühn, C., Bleiss, W., Giavalisco, P., Willmitzer, L., et al. (2009). RNA interference of *LIN5* in tomato confirms its role in controlling Brix content, uncovers the influence of sugars on the levels of fruit hormones, and demonstrates the importance of sucrose cleavage for normal fruit development and fertility. Plant Physiol. *150*, 1204–1218. https://doi.org/10.1104/pp.109.136598.
23. Cheng, W.H., Taliercio, E.W., and Chourey, P.S. (1996). The *MINIATURE1* seed locus of maize encodes a cell wall invertase required for normal development of endosperm and maternal cells in the pedicel. Plant Cell *8*, 971–983. https://doi.org/10.1105/tpc.8.6.971.
24. Pressman, E., Peet, M.M., and Pharr, D.M. (2002). The effect of heat stress on tomato pollen characteristics is associated with changes in

carbohydrate concentration in the developing anthers. Ann. Bot. *90*, 631–636. https://doi.org/10.1093/aob/mcf240.

25. Rizhsky, L., Liang, H., Shuman, J., Shulaev, V., Davletova, S., and Mittler, R. (2004). When defense pathways collide. The response of *Arabidopsis* to a combination of drought and heat stress. Plant Physiol. *134*, 1683–1696. https://doi.org/10.1104/pp.103.033431.
26. Suwa, R., Hakata, H., Hara, H., El-Shemy, H.A., Adu-Gyamfi, J.J., Nguyen, N.T., Kanai, S., Lightfoot, D.A., Mohapatra, P.K., and Fujita, K. (2010). High temperature effects on photosynthate partitioning and sugar metabolism during ear expansion in maize (*Zea mays L.*) genotypes. Plant Physiol. Biochem. *48*, 124–130. https://doi.org/10.1016/j.plaphy.2009.12.010.
27. Liu, Y.H., Offler, C.E., and Ruan, Y.L. (2013). Regulation of fruit and seed response to heat and drought by sugars as nutrients and signals. Front. Plant Sci. *4*, 282. https://doi.org/10.3389/fpls.2013.00282.
28. Rodriguez-Leal, D., Xu, C., Kwon, C.T., Soyars, C., Demesa-Arevalo, E., Man, J., Liu, L., Lemmon, Z.H., Jones, D.S., Van Eck, J., et al. (2019). Evolution of buffering in a genetic circuit controlling plant stem cell proliferation. Nat. Genet. *51*, 786–792. https://doi.org/10.1038/s41588-019-0389-8.
29. Amthor, J.S. (2000). The mccree–de wit–penning de vries–thornley respiration paradigms: 30 years later. Ann. Bot. *86*, 1–20. https://doi.org/10.1006/anbo.2000.1175.
30. von Schaewen, A., Stitt, M., Schmidt, R., Sonnewald, U., and Willmitzer, L. (1990). Expression of a yeast-derived invertase in the cell wall of tobacco and *Arabidopsis* plants leads to accumulation of carbohydrate and inhibition of photosynthesis and strongly influences growth and phenotype of transgenic tobacco plants. EMBO J. *9*, 3033–3044. https://doi.org/10.1002/j.1460-2075.1990.tb07499.x.
31. Dickinson, C.D., Altabella, T., and Chrispeels, M.J. (1991). Slow-growth phenotype of transgenic tomato expressing apoplastic invertase. Plant Physiol. *95*, 420–425. https://doi.org/10.1104/pp.95.2.420.
32. Ismail, A.M., and Hall, A.E. (1999). Reproductive-stage heat tolerance, leaf membrane thermostability and plant morphology in cowpea. Crop Sci. *39*, 1762–1768. https://doi.org/10.2135/cropsci1999.3961762x.
33. Peng, S., Huang, J., Sheehy, J.E., Laza, R.C., Visperas, R.M., Zhong, X., Centeno, G.S., Khush, G.S., and Cassman, K.G. (2004). Rice yields decline with higher night temperature from global warming. Proc. Natl. Acad. Sci. USA *101*, 9971–9975. https://doi.org/10.1073/pnas.0403720101.
34. Cox, D.T.C., Maclean, I.M.D., Gardner, A.S., and Gaston, K.J. (2020). Global variation in diurnal asymmetry in temperature, cloud cover, specific humidity and precipitation and its association with leaf area index. Glob. Chang. Biol. *26*, 7099–7111. https://doi.org/10.1111/gcb.15336.
35. Riesmeier, J.W., Willmitzer, L., and Frommer, W.B. (1994). Evidence for an essential role of the sucrose transporter in phloem loading and assimilate partitioning. EMBO J. *13*, 1–7. https://doi.org/10.1002/j.1460-2075.1994.tb06229.x.
36. Chourey, P.S., Taliercio, E.W., Carlson, S.J., and Ruan, Y.L. (1998). Genetic evidence that the two isozymes of sucrose synthase present in developing maize endosperm are critical, one for cell wall integrity and the other for starch biosynthesis. Mol. Gen. Genet. *259*, 88–96. https://doi.org/10.1007/s004380050792.
37. Micallef, B.J., Haskins, K.A., Vanderveer, P.J., Roh, K.-S., Shewmaker, C.K., and Sharkey, T.D. (1995). Altered photosynthesis, flowering, and fruiting in transgenic tomato plants that have an increased capacity for sucrose synthesis. Planta *196*, 327–334. https://doi.org/10.1007/BF00201392.
38. Wang, Z., Wei, K., Xiong, M., Wang, J.-D., Zhang, C.-Q., Fan, X.-L., Huang, L.-C., Zhao, D.-S., Liu, Q.-Q., and Li, Q.-F. (2021). GLUCAN, WATER-DIKINASE 1 (GWD1), an ideal biotechnological target for potential improving yield and quality in rice. Plant Biotechnol. J. *19*, 2606–2618. https://doi.org/10.1111/pbi.13686.
39. Bonner, J.J., Ballou, C., and Fackenthal, D.L. (1994). Interactions between DNA-bound trimers of the yeast heat shock factor. Mol. Cell. Biol. *14*, 501–508. https://doi.org/10.1128/mcb.14.1.501-508.1994.
40. Waters, E.R. (1995). The molecular evolution of the small heat-shock proteins in plants. Genetics *141*, 785–795. https://doi.org/10.1093/genetics/141.2.785.
41. Richter, K., Haslbeck, M., and Buchner, J. (2010). The heat shock response: life on the verge of death. Mol. Cell *40*, 253–266. https://doi.org/10.1016/j.molcel.2010.10.006.
42. Xiao, H., and Lis, J.T. (1988). Germline transformation used to define key features of heat-shock response elements. Science *239*, 1139–1142. https://doi.org/10.1126/science.3125608.
43. Suzuki, N., Sejima, H., Tam, R., Schlauch, K., and Mittler, R. (2011). Identification of the MBF1 heat-response regulon of *Arabidopsis thaliana*. Plant J. *66*, 844–851. https://doi.org/10.1111/j.1365-313X.2011.04550.x.
44. Fragkostefanakis, S., Simm, S., Paul, P., Bublak, D., Scharf, K.D., and Schleiff, E. (2015). Chaperone network composition in *Solanum lycopersicum* explored by transcriptome profiling and microarray meta-analysis. Plant Cell Environ. *38*, 693–709. https://doi.org/10.1111/pce.12426.
45. Arce, D., Spetale, F., Krsticevic, F., Cacchiarelli, P., Las Rivas, J.D., Ponce, S., Pratta, G., and Tapia, E. (2018). Regulatory motifs found in the *SMALL HEAT SHOCK PROTEIN* (*sHSP*) gene family in tomato. BMC Genom. *19*, 860. https://doi.org/10.1186/s12864-018-5190-z.
46. Lü, P., Yu, S., Zhu, N., Chen, Y.-R., Zhou, B., Pan, Y., Tzeng, D., Fabi, J.P., Argyris, J., Garcia-Mas, J., et al. (2018). Genome encode analyses reveal the basis of convergent evolution of fleshy fruit ripening. Nat. Plants *4*, 784–791. https://doi.org/10.1038/s41477-018-0249-z.
47. Dunwell, J.M. (2000). Transgenic approaches to crop improvement. J. Exp. Bot. *51*, 487–496. https://doi.org/10.1093/jexbot/51.suppl_1.487.
48. Vaucheret, H., Béclin, C., Elmayan, T., Feuerbach, F., Godon, C., Morel, J.B., Mourrain, P., Palauqui, J.C., and Vernhettes, S. (1998). Transgene-induced gene silencing in plants. Plant J. *16*, 651–659. https://doi.org/10.1046/j.1365-313x.1998.00337.x.
49. Lu, Y., Tian, Y., Shen, R., Yao, Q., Zhong, D., Zhang, X., and Zhu, J.K. (2021). Precise genome modification in tomato using an improved prime editing system. Plant Biotechnol. J. *19*, 415–417. https://doi.org/10.1111/pbi.13497.
50. Vu, T.V., Nguyen, N.T., Kim, J., Hong, J.C., and Kim, J.Y. (2024). Prime editing: mechanism insight and recent applications in plants. Plant Biotechnol. J. *22*, 19–36. https://doi.org/10.1111/pbi.14188.
51. Liu, Y., Yang, G., Huang, S., Li, X., Wang, X., Li, G., Chi, T., Chen, Y., Huang, X., and Wang, X. (2021). Enhancing prime editing by Csy4-mediated processing of pegRNA. Cell Res. *31*, 1134–1136. https://doi.org/10.1038/s41422-021-00520-x.
52. Nelson, J.W., Randolph, P.B., Shen, S.P., Everette, K.A., Chen, P.J., Anzalone, A.V., An, M., Newby, G.A., Chen, J.C., Hsu, A., et al. (2022). Engineered pegRNAs improve prime editing efficiency. Nat. Biotechnol. *40*, 402–410. https://doi.org/10.1038/s41587-021-01039-7.
53. Sternberg, S.H., Haurwitz, R.E., and Doudna, J.A. (2012). Mechanism of substrate selection by a highly specific CRISPR endoribonuclease. RNA *18*, 661–672. https://doi.org/10.1261/rna.030882.111.
54. Stavolone, L., Kononova, M., Pauli, S., Ragozzino, A., de Haan, P., Milligan, S., Lawton, K., and Hohn, T. (2003). Cestrum yellow leaf curling virus (*CmYLCV*) promoter: a new strong constitutive promoter for heterologous gene expression in a wide variety of crops. Plant Mol. Biol. *53*, 663–673. https://doi.org/10.1023/B:PLAN.0000019110.95420.bb.
55. Xie, K., Minkenberg, B., and Yang, Y. (2015). Boosting CRISPR/Cas9 multiplex editing capability with the endogenous tRNA-processing system. Proc. Natl. Acad. Sci. USA *112*, 3570–3575. https://doi.org/10.1073/pnas.1420294112.
56. Hong, C., Han, J.H., Hwang, G.H., Bae, S., and Seo, P.J. (2024). Genome-wide in-locus epitope tagging of *Arabidopsis* proteins using

prime editors. BMB Rep. *57*, 66–70. https://doi.org/10.5483/BMBRep.2023-0055.

57. Vats, S., Kumar, J., Sonah, H., Zhang, F., and Deshmukh, R. (2024). Prime editing in plants: prospects and challenges. J. Exp. Bot. *75*, 5344–5356. https://doi.org/10.1093/jxb/erae053.

58. Vu, T.V., Nguyen, N.T., Kim, J., Song, Y.J., Nguyen, T.H., and Kim, J.Y. (2024). Optimized dicot prime editing enables heritable desired edits in tomato and *Arabidopsis*. Nat. Plants *10*, 1502–1513. https://doi.org/10.1038/s41477-024-01786-w.

59. Osorio, S., Ruan, Y.L., and Fernie, A.R. (2014). An update on source-to-sink carbon partitioning in tomato. Front. Plant Sci. *5*, 516. https://doi.org/10.3389/fpls.2014.00516.

60. Chang, T.G., Zhu, X.G., and Raines, C. (2017). Source-sink interaction: a century old concept under the light of modern molecular systems biology. J. Exp. Bot. *68*, 4417–4431. https://doi.org/10.1093/jxb/erx002.

61. Körner, C. (2015). Paradigm shift in plant growth control. Curr. Opin. Plant Biol. *25*, 107–114. https://doi.org/10.1016/j.pbi.2015.05.003.

62. Paul, M.J., and Foyer, C.H. (2001). Sink regulation of photosynthesis. J. Exp. Bot. *52*, 1383–1400. https://doi.org/10.1093/jexbot/52.360.1383.

63. Zhang, C., Wang, J., Wang, X., Li, C., Ye, Z., and Zhang, J. (2020). *UF*, a WOX gene, regulates a novel phenotype of un-fused flower in tomato. Plant Sci. *297*, 110523. https://doi.org/10.1016/j.plantsci.2020.110523.

64. Chakrabarti, M., Zhang, N., Sauvage, C., Muños, S., Blanca, J., Cañizares, J., Diez, M.J., Schneider, R., Mazourek, M., McClead, J., et al. (2013). A cytochrome P450 regulates a domestication trait in cultivated tomato. Proc. Natl. Acad. Sci. USA *110*, 17125–17130. https://doi.org/10.1073/pnas.1307313110.

65. Yang, T., He, Y., Niu, S., and Zhang, Y. (2022). A YABBY gene *CRABS CLAW a* (*CRCa*) negatively regulates flower and fruit sizes in tomato. Plant Sci. *320*, 111285. https://doi.org/10.1016/j.plantsci.2022.111285.

66. Sun, L., Yang, D.L., Kong, Y., Chen, Y., Li, X.Z., Zeng, L.J., Li, Q., Wang, E.T., and He, Z.H. (2014). Sugar homeostasis mediated by cell wall invertase GRAIN INCOMPLETE FILLING 1 (GIF1) plays a role in pre-existing and induced defence in rice. Mol. Plant Pathol. *15*, 161–173. https://doi.org/10.1111/mpp.12078.

67. Wei, X., Chen, M., Zhang, Q., Gong, J., Liu, J., Yong, K., Wang, Q., Fan, J., Chen, S., Hua, H., et al. (2024). Genomic investigation of 18,421 lines reveals the genetic architecture of rice. Science *385*, eadm8762. https://doi.org/10.1126/science.adm8762.

68. Ma, X., Zhang, Q., Zhu, Q., Liu, W., Chen, Y., Qiu, R., Wang, B., Yang, Z., Li, H., Lin, Y., et al. (2015). A robust CRISPR/Cas9 system for convenient, high-efficiency multiplex genome editing in monocot and dicot plants. Mol. Plant *8*, 1274–1284. https://doi.org/10.1016/j.molp.2015.04.007.

69. Song, X., Meng, X., Guo, H., Cheng, Q., Jing, Y., Chen, M., Liu, G., Wang, B., Wang, Y., Li, J., et al. (2022). Targeting a gene regulatory element enhances rice grain yield by decoupling panicle number and size. Nat. Biotechnol. *40*, 1403–1411. https://doi.org/10.1038/s41587-022-01281-7.

70. Zhang, H., Zhou, J.-F., Kan, Y., Shan, J.-X., Ye, W.-W., Dong, N.-Q., Guo, T., Xiang, Y.-H., Yang, Y.-B., Li, Y.-C., et al. (2022). A genetic module at one locus in rice protects chloroplasts to enhance thermotolerance. Science *376*, 1293–1300. https://doi.org/10.1126/science.abo5721.

71. Seki, M., Feugier, F.G., Song, X.J., Ashikari, M., Nakamura, H., Ishiyama, K., Yamaya, T., Inari-Ikeda, M., Kitano, H., and Satake, A. (2015). A mathematical model of phloem sucrose transport as a new tool for designing rice panicle structure for high grain yield. Plant Cell Physiol. *56*, 605–619. https://doi.org/10.1093/pcp/pcu191.

72. Lauxmann, M.A., Annunziata, M.G., Brunoud, G., Wahl, V., Koczut, A., Burgos, A., Olas, J.J., Maximova, E., Abel, C., Schlereth, A., et al. (2016). Reproductive failure in *Arabidopsis thaliana* under transient carbohydrate limitation: flowers and very young siliques are jettisoned and the meristem is maintained to allow successful resumption of reproductive growth. Plant Cell Environ. *39*, 745–767. https://doi.org/10.1111/pce.12634.

73. Lemoine, R., La Camera, S., Atanassova, R., Dédaldéchamp, F., Allario, T., Pourtau, N., Bonnemain, J.L., Laloi, M., Coutos-Thévenot, P., Maurousset, L., et al. (2013). Source-to-sink transport of sugar and regulation by environmental factors. Front. Plant Sci. *4*, 272. https://doi.org/10.3389/fpls.2013.00272.

74. Smith, M.R., Rao, I.M., and Merchant, A. (2018). Source-sink relationships in crop plants and their influence on yield development and nutritional quality. Front. Plant Sci. *9*, 1889. https://doi.org/10.3389/fpls.2018.01889.

75. Li, B., Liu, H., Zhang, Y., Kang, T., Zhang, L., Tong, J., Xiao, L., and Zhang, H. (2013). Constitutive expression of cell wall invertase genes increases grain yield and starch content in maize. Plant Biotechnol. J. *11*, 1080–1091. https://doi.org/10.1111/pbi.12102.

76. Nam, H., Gupta, A., Nam, H., Lee, S., Cho, H.S., Park, C., Park, S., Park, S.J., and Hwang, I. (2022). JULGI-mediated increment in phloem transport capacity relates to fruit yield in tomato. Plant Biotechnol. J. *20*, 1533–1545. https://doi.org/10.1111/pbi.13831.

77. Singh, J., Das, S., Jagadis Gupta, K., Ranjan, A., Foyer, C.H., and Thakur, J.K. (2023). Physiological implications of SWEETs in plants and their potential applications in improving source-sink relationships for enhanced yield. Plant Biotechnol. J. *21*, 1528–1541. https://doi.org/10.1111/pbi.13982.

78. Rodríguez-Leal, D., Lemmon, Z.H., Man, J., Bartlett, M.E., and Lippman, Z.B. (2017). Engineering quantitative trait variation for crop improvement by genome editing. Cell *171*, 470–480.e8. https://doi.org/10.1016/j.cell.2017.08.030.

79. Soyk, S., Lemmon, Z.H., Oved, M., Fisher, J., Liberatore, K.L., Park, S.J., Goren, A., Jiang, K., Ramos, A., van der Knaap, E., et al. (2017). Bypassing negative epistasis on yield in tomato imposed by a domestication gene. Cell *169*, 1142–1155.e12. https://doi.org/10.1016/j.cell.2017.04.032.

80. Xu, G., Yuan, M., Ai, C., Liu, L., Zhuang, E., Karapetyan, S., Wang, S., and Dong, X. (2017). uORF-mediated translation allows engineered plant disease resistance without fitness costs. Nature *545*, 491–494. https://doi.org/10.1038/nature22372.

81. Mendieta, J.P., Sangra, A., Yan, H., Minow, M.A.A., and Schmitz, R.J. (2023). Exploring plant *cis*-regulatory elements at single-cell resolution: overcoming biological and computational challenges to advance plant research. Plant J. *115*, 1486–1499. https://doi.org/10.1111/tpj.16351.

82. Li, T., Yang, X., Yu, Y., Si, X., Zhai, X., Zhang, H., Dong, W., Gao, C., and Xu, C. (2018). Domestication of wild tomato is accelerated by genome editing. Nat. Biotechnol. *36*, 1160–1163. https://doi.org/10.1038/nbt.4273.

83. Xu, C., Wang, Y., Yu, Y., Duan, J., Liao, Z., Xiong, G., Meng, X., Liu, G., Qian, Q., and Li, J. (2012). Degradation of MONOCULM 1 by APC/CTAD1 regulates rice tillering. Nat. Commun. *3*, 750. https://doi.org/10.1038/ncomms1743.

84. Čermák, T., Curtin, S.J., Gil-Humanes, J., Čegan, R., Kono, T.J.Y., Konečná, E., Belanto, J.J., Starker, C.G., Mathre, J.W., Greenstein, R.L., et al. (2017). A multipurpose toolkit to enable advanced genome engineering in plants. Plant Cell *29*, 1196–1217. https://doi.org/10.1105/tpc.16.00922.

85. Hellens, R.P., Allan, A.C., Friel, E.N., Bolitho, K., Grafton, K., Templeton, M.D., Karunairetnam, S., Gleave, A.P., and Laing, W.A. (2005). Transient expression vectors for functional genomics, quantification of promoter activity and RNA silencing in plants. Plant Methods *1*, 13. https://doi.org/10.1186/1746-4811-1-13.

86. Huang, X., Chen, S., Li, W., Tang, L., Zhang, Y., Yang, N., Zou, Y., Zhai, X., Xiao, N., Liu, W., et al. (2021). ROS regulated reversible protein phase separation synchronizes plant flowering. Nat. Chem. Biol. *17*, 549–557. https://doi.org/10.1038/s41589-021-00739-0.

87. Kumar, S., Stecher, G., Li, M., Knyaz, C., and Tamura, K. (2018). MEGA X: molecular evolutionary genetics analysis across computing platforms. Mol. Biol. Evol. *35*, 1547–1549. https://doi.org/10.1093/molbev/msy096.

88. Bailey, T.L., Boden, M., Buske, F.A., Frith, M., Grant, C.E., Clementi, L., Ren, J., Li, W.W., and Noble, W.S. (2009). MEME Suite: tools for motif discovery and searching. Nucleic Acids Res. *37*, W202–W208. https://doi.org/10.1093/nar/gkp335.

89. Bae, S., Park, J., and Kim, J.S. (2014). Cas-OFFinder: a fast and versatile algorithm that searches for potential off-target sites of Cas9 RNA-guided endonucleases. Bioinformatics Oxf. Engl. *30*, 1473–1475. https://doi.org/10.1093/bioinformatics/btu048.

90. Lescot, M., Déhais, P., Thijs, G., Marchal, K., Moreau, Y., Van de Peer, Y., Rouzé, P., and Rombauts, S. (2002). PlantCARE, a database of plant *cis*-acting regulatory elements and a portal to tools for in silico analysis of promoter sequences. Nucleic Acids Res. *30*, 325–327. https://doi.org/10.1093/nar/30.1.325.

91. McGinnis, S., and Madden, T.L. (2004). BLAST: at the core of a powerful and diverse set of sequence analysis tools. Nucleic Acids Res. *32*, W20–W25. https://doi.org/10.1093/nar/gkh435.

92. Frazer, K.A., Pachter, L., Poliakov, A., Rubin, E.M., and Dubchak, I. (2004). VISTA: computational tools for comparative genomics. Nucleic Acids Res. *32*, W273–W279. https://doi.org/10.1093/nar/gkh458.

93. Waterhouse, A., Procter, J., Martin, D.A., and Barton, G.J. (2005). Jalview: visualization and analysis of molecular sequences, alignments, and structures. BMC Bioinform. *6*, 28. https://doi.org/10.1186/1471-2105-6-S3-P28.

94. Bolger, A.M., Lohse, M., and Usadel, B. (2014). Trimmomatic: a flexible trimmer for Illumina sequence data. Bioinformatics Oxf. Engl. *30*, 2114–2120. https://doi.org/10.1093/bioinformatics/btu170.

95. Kim, D., Langmead, B., and Salzberg, S.L. (2015). HISAT: a fast spliced aligner with low memory requirements. Nat. Methods *12*, 357–360. https://doi.org/10.1038/nmeth.3317.

96. Li, H., Handsaker, B., Wysoker, A., Fennell, T., Ruan, J., Homer, N., Marth, G., Abecasis, G., and Durbin, R.; 1000 Genome Project Data Processing Subgroup (2009). The sequence alignment/map format and SAMtools. Bioinformatics Oxf. Engl. *25*, 2078–2079. https://doi.org/10.1093/bioinformatics/btp352.

97. Pertea, M., Pertea, G.M., Antonescu, C.M., Chang, T.C., Mendell, J.T., and Salzberg, S.L. (2015). StringTie enables improved reconstruction of a transcriptome from RNA-seq reads. Nat. Biotechnol. *33*, 290–295. https://doi.org/10.1038/nbt.3122.

98. Tian, T., Liu, Y., Yan, H., You, Q., Yi, X., Du, Z., Xu, W., and Su, Z. (2017). AgriGO v2.0: a GO analysis toolkit for the agricultural community, 2017 update. Nucleic Acids Res. *45*, W122–W129. https://doi.org/10.1093/nar/gkx382.

99. Allen, G.C., Flores-Vergara, M.A., Krasynanski, S., Kumar, S., and Thompson, W.F. (2006). A modified protocol for rapid DNA isolation from plant tissues using cetyltrimethylammonium bromide. Nat. Protoc. *1*, 2320–2325. https://doi.org/10.1038/nprot.2006.384.

100. Jin, S., Zong, Y., Gao, Q., Zhu, Z., Wang, Y., Qin, P., Liang, C., Wang, D., Qiu, J.L., Zhang, F., et al. (2019). Cytosine, but not adenine, base editors induce genome-wide off-target mutations in rice. Science *364*, 292–295. https://doi.org/10.1126/science.aaw7166.

101. Alexander, M.P. (1969). Differential staining of aborted and nonaborted pollen. Stain Technol. *44*, 117–122. https://doi.org/10.3109/10520296909063335.

102. Paupière, M.J., Müller, F., Li, H., Rieu, I., Tikunov, Y.M., Visser, R.G.F., and Bovy, A.G. (2017). Untargeted metabolomic analysis of tomato pollen development and heat stress response. Plant Reprod. *30*, 81–94. https://doi.org/10.1007/s00497-017-0301-6.

103. Begcy, K., Nosenko, T., Zhou, L.Z., Fragner, L., Weckwerth, W., and Dresselhaus, T. (2019). Male sterility in maize after transient heat stress during the tetrad stage of pollen development. Plant Physiol. *181*, 683–700. https://doi.org/10.1104/pp.19.00707.

104. Shang, L., Li, X., He, H., Yuan, Q., Song, Y., Wei, Z., Lin, H., Hu, M., Zhao, F., Zhang, C., et al. (2022). A super pan-genomic landscape of rice. Cell Res. *32*, 878–896. https://doi.org/10.1038/s41422-022-00685-z.

105. Wang, Y., Li, F., Zhang, F., Wu, L., Xu, N., Sun, Q., Chen, H., Yu, Z., Lu, J., Jiang, K., et al. (2023). Time-ordering japonica/geng genomes analysis indicates the importance of large structural variants in rice breeding. Plant Biotechnol. J. *21*, 202–218. https://doi.org/10.1111/pbi.13938.

106. Qin, P., Lu, H., Du, H., Wang, H., Chen, W., Chen, Z., He, Q., Ou, S., Zhang, H., Li, X., et al. (2021). Pan-genome analysis of 33 genetically diverse rice accessions reveals hidden genomic variations. Cell *184*, 3542–3558.e16. https://doi.org/10.1016/j.cell.2021.04.046.

Please cite this article in press as: Lou et al., Engineering source-sink relations by prime editing confers heat-stress resilience in tomato and rice, Cell (2025), https://doi.org/10.1016/j.cell.2024.11.005

STAR★METHODS

KEY RESOURCES TABLE

REAGENT or RESOURCE	SOURCE	IDENTIFIER
Bacterial and virus strains		
Agrobacterium tumefaciens strain AGL1	Li et al.[82]	N/A
Agrobacterium tumefaciens strain EHA105	Xu et al.[83]	N/A
Agrobacterium tumefaciens strain GV3101	WEIDI	Cat# AC1003L
Biological samples		
DNA and RNA from various plant tissues from tomato and rice	See STAR Methods	N//A
Chemicals, peptides, and recombinant proteins		
CTAB	N/A	N/A
Agarose	BIOWESTE	Cat# 111860
BsaI	NEB	Cat# R0535L
T4 DNA Ligase	NEB	Cat# M0202L
XbaI	NEB	Cat# R0145
KODone	TOYOBO	Cat# KMM-101
TRIZOL	Invitrogen	Cat# 15596018
Ultra Taq PCR StarMix	GenStar	Cat# ZA019-101S
[^{14}C (U)] Sucrose	Moravek	Cat# MC266
Critical commercial assays		
ClonExpress II one Step Cloning Kit	Vazyme	Cat# C115
Dual-Luciferase Reporter Assay System	Promega	Cat#E1910
Fastking RT Kit (With gDNase)	TIANGEN	Cat# KR116
TB Green Premix Ex Taq II	TAKARA	Cat# RR820
TURBO DNA-free Kit	Invitrogen	Cat# AM1907
Matchmaker™ Gold Yeast One-Hybrid System	Clontech	Cat# 630491, 630466, 630499
Deposited data		
RNAseq data	This paper	GSA: PRJCA024921
Experimental models: Organisms/strains		
Solanum lycopersicum cv. Micro-Tom, MT	This paper	N/A
Solanum lycopersicum cv. Ailsa Craig, AC	This paper	N/A
Solanum lycopersicum cv. M82	This paper	N/A
Solanum lycopersicum cv. Yuanwei-1, YW1	This paper	N/A
Tomato: *lin5^{CR}-a1*	This paper	N/A
Tomato: *lin5^{CR}-a2*	This paper	N/A
Tomato: *35Spro:LIN5-1*	This paper	N/A
Tomato: *35Spro:LIN5-5*	This paper	N/A
Tomato: *lin5-de*	This paper	N/A
Tomato: ac-*lin5-de*	This paper	N/A
Tomato: *m82-lin5-de*	This paper	N/A
Tomato: *yw1-lin5-de*	This paper	N/A
Oryza sativa L. spp. *Japonica* Zhonghua11, ZH11	This paper	N/A
Oryza sativa L. spp. *Japonica* Wuyoudao-4, WYD-4	This paper	N/A
Oryza sativa L. spp. *Japonica* Zhongkefa-5	This paper	N/A
Oryza sativa L. spp. *Japonica* Longgeng-31	This paper	N/A

(*Continued on next page*)

Please cite this article in press as: Lou et al., Engineering source-sink relations by prime editing confers heat-stress resilience in tomato and rice, Cell (2025), https://doi.org/10.1016/j.cell.2024.11.005

Continued

REAGENT or RESOURCE	SOURCE	IDENTIFIER
Rice: *gif1-de*	This paper	N/A
Rice: *wyd-4-gif1-de*	This paper	N/A
Nicotiana benthamiana	This paper	N/A
Oligonucleotides		
Primers listed in Table S5	BGI (Beijing, China)	Custom order
Recombinant DNA		
pDIRECT-22C-lin5^{CR}	This paper	N/A
pRI101-35S$_{pro}$:LIN5	This paper	N/A
pGreenII0800-LIN5$_{pro}$	This paper	N/A
pGreenII0800-LIN5$_{pro+HSE}$	This paper	N/A
pGreenII0800-LIN5$_{pro+HSE\ scram}$	This paper	N/A
U6-PE-LIN5	This paper	N/A
tRNA-PE-LIN5	This paper	N/A
Csy4-PE-LIN5	This paper	N/A
Csy4-PE-FLAVIN MONOOXYGENASE	This paper	N/A
Csy4-PE-ERRECTA	This paper	N/A
pCAM-PE-GIF1	This paper	N/A
pDIRECT-22C	Cermak et al.[84]	Addgene #91135
pGreenII0800-LUC	Hellens et al.[85]	N/A
pYLCRISPR/Cas9P$_{ubi}$-H	Ma et al.[68]	Addgene #66187
pRI101 vector	Huang et al.[86]	N/A
Csy4-PE	This paper	N/A
pCAM-PE	This paper	N/A
Software and algorithms		
MEGA X	Kumar et al.[87]	https://www.megasoftware.net/
The MEME Suite	Bailey et al.[88]	https://meme-suite.org/meme/
Cas-OFFinder	Bae et al.[89]	http://www.rgenome.net/cas-offinder/
PlantCARE	Lescot et al.[90]	http://bioinformatics.psb.ugent.be/webtools/plantcare/html/
fruitENCODE	Lü et al.[46]	www.epigenome.cuhk.edu.hk/encode.html
NCBI BLAST	McGinnis et al.[91]	http://www.ncbi.nlm.nih.gov/BLAST/
mVISTA	Frazer et al.[92]	http://genome.lbl.gov/vista/mvista/submit.shtml
Jalview	Waterhouse et al.[93]	https://www.jalview.org/
Trimmomatic (v0.36)	Bolger et al.[94]	https://github.com/usadellab/Trimmomatic
Hisat2 (v2.1.0)	Kim et al.[95]	https://github.com/DaehwanKimLab/hisat2
Samtools (v1.8)	Li et al.[96]	https://github.com/samtools/samtools
StringTie (v 2.0.3)	Pertea et al.[97]	https://github.com/gpertea/stringtie
AgriGO (V2.0)	Tian et al.[98]	https://systemsbiology.cau.edu.cn/agriGOv2/

Experimental model and study participant details

Plant materials and growth conditions

Tomato (*Solanum lycopersicum*) cultivars Micro-Tom, Ailsa Craig, M82 and Yuanwei-1 were used in this study. Micro-Tom is a dwarf and compact variety suited for growing under controlled conditions that produces 'cherry' fruit and is readily transformed. Ailsa Craig tomato variety is cultivated for greenhouse production and is known for its taste and flavor, traditionally used in English breakfasts and cultivated by amateur home gardeners. Now, it has been an experimental staple of tomato molecular biology and biotechnology. M82 is a processed tomato variety and Yuanwei-1 is a modern fresh tomato inbred line. Seeds were directly sown in soil in 72-cell plastic flat trays. Seedlings with 3–4 true leaves were transplanted to pots and either were grown in an artificial climate room (25°C/23°C day/night) equipped with LED lights (Philips Lighting IBRS, 10461, 5600 VB, NL) under long-day conditions (16-h light/8-h dark) or in a greenhouse under natural light.

The elite rice *japonica* cultivar Zhonghua 11 and Wuyoudao-4 were used for genetic transformation in this study. We also selected two recently approved and widely planted elite rice varieties namely Longgeng-31 and Zhongkefa-5, to analyze expression of *GIF1* under normal and heat stress conditions. For seedling preparation, seeds were pre-germinated on filter paper irrigated with distilled water and subsequently sown in soil in 72-well plastic flat trays. Seedlings were then grown for 1 month before transplanting into the field. Rice plants were cultivated in experimental fields in Beijing, China (N 39.9°, E 116.3°) from May to October in 2023, and in Hainan, China (N 110.1°, E 18.5°) from December 2023 to March 2024. The cultivation and management practices for tomato and rice are consistent with those used by local farms, including planting density, fertilizer application, tilling, irrigation, sowing and harvesting.

Nicotiana benthamiana was used for dual-luciferase reporter assays. Plants were germinated from seed, propagated in soil and grown under controlled environmental conditions equipped with LED lights at a constant temperature of 25°C with a 16-h light and 8-h dark photoperiod. The top three well-expanded leaves of three independent plants (approximately 6–8 weeks old) were infiltrated with Agrobacteria GV3101 (pSoup-p19) (CAT# AC1003L) harboring each vector or vector combinations. Agrobacteria were delivered into the underside of leaves using a blunt tipped plastic syringe and applying gentle pressure.

METHOD DETAILS

Heat-stress experiments and data collection

Short-term heat treatment on tomato c.v. Micro-Tom

After transplanting, seedlings were grown in an artificial climate room (16 h illumination at 25°C/8 h darkness at 22°C; 40–60% relative humidity) equipped with LED lights at 140 μmol m^{-2} s^{-1} light intensity. After the last flower on the first inflorescence had fully bloomed, all plants were subjected to heat treatment in a growth chamber (Conviron CMP6010) for 14 d (16 h illumination at 40°C/8 h darkness at 30°C; 50% relative humidity). Heat-treated plants were then returned to the artificial climate room until the first and second trusses of fruits ripened for phenotypic scoring.

Normal growth condition of solar greenhouse for tomato c.v. Micro-Tom

After transplanting, plants were grown in a plastic solar greenhouse with natural lighting at 28°C daytime/19°C nighttime for 70 days until the first and second trusses of fruits reached maturity for phenotypic scoring. Temperature changes during growth were monitored in real-time using sensors.

Long-term heat-stress treatment on tomato c.v. Micro-Tom

By taking advantage of the high-temperature weather during the summer in Beijing (19 June 2022 to 19 August 2022) and natural light, plants were grown in pots in a plastic solar greenhouse (33°C daytime/28.5°C nighttime) for 60 days after transplanting until the first and second trusses of fruits ripened for phenotypic scoring. Temperature changes during tomato growth were monitored in real-time using sensors.

Long-term heat-stress treatment on tomato c.v. Ailsa Craig.

Ailsa Craig seedlings were transplanted directly into the soil within a plastic solar greenhouse with natural lighting and 32°C daytime/21°C nighttime temperatures for 50 days. After the last flower on the first inflorescence had just set fruit, plants were covered with an additional layer of transparent plastic film to create a high-temperature microenvironment, the bottom of which was kept open for airflow. After the first and second trusses of fruits were fully ripened, phenotypes were scored. Temperature changes during growth were monitored in real-time using sensors.

Heat stress for tomato c.v. Ailsa Craig in an open field

After the last flower on the first inflorescence had just set fruit, plants were covered with a layer of transparent plastic film to create a high-temperature microenvironment of 38°C daytime/24°C nighttime for 36 d, the bottom of which was kept open for airflow. These plants grew without any artificial interventions such as pruning or trellising, apart from regular watering. After the first and second trusses of fruits were fully ripened, phenotypes were scored. The temperature changes during tomato growth were monitored in real-time using sensors.

Longer-term higher temperature growth for yield trial in solar greenhouse

To take advantage of natural high temperature in summer season in Beijing (May 2024 to June 2024) for yield analysis, we delayed the sowing by one month compared to the normal planting time, allowing the tomato seedlings to catch up with the summer high temperature. By monitoring with temperature sensors, this method led to an increase of 4°C in the average daytime temperature and 6°C in the nighttime temperature during 30 d following flowering.

Rice heat stress in a paddy field

After transplanting into the paddy field, wild-type c.v. ZH11 plants and corresponding mutants were grown until heading stage. During this period, the outside daytime temperature was about 30.5°C and the nighttime temperature was about 21.5°C. To increase the temperature, rice plants were covered with a layer of transparent plastic film with the bottom kept open for airflow. The average temperature reached 36°C during the daytime and 24°C at night. Fully mature panicles were harvested for yield analysis. Temperature changes during growth were monitored in real-time using sensors.

Please cite this article in press as: Lou et al., Engineering source-sink relations by prime editing confers heat-stress resilience in tomato and rice, Cell (2025), https://doi.org/10.1016/j.cell.2024.11.005

Fruit and grain yield evaluation

All yield trials of prime-edited tomato and rice plants conducted in greenhouse or field settings use transgene-free homozygous mutant materials. For yield evaluation of c.v. Micro-Tom, one plant was grown per pot. Fruit yields under different conditions were calculated as the total fresh weight of all fruits on the first two inflorescences from each plant. The number of plants used for yield quantification is specified in the respective figure legends.

For yield evaluation of c.v. Ailsa Craig grown in a plastic solar greenhouse at different locations, fruit yield was estimated by excluding edge plants and grouping four tomato plants per m^2 as one plot. Four, eight, or ten plots for fruit yield were used for statistical analyses. The total fresh weight of all fruits from the first three inflorescences was considered as the yield of each plot. To score the traits of average fruit fresh weight per inflorescence, average Brix index per inflorescence, fruit-set rate and harvest index, random sampling was performed on the plants grown for yield trials with excluding the edge plants. The harvest index is defined as the ratio of the total fresh fruit weight to the total weight of the plant biomass aboveground.

For evaluation of Ailsa Craig plants in open fields, yield was estimated by grouping 3 plants per m^2 as one plot, and the total fresh weight of all fruits on the tomato plants in each plot was considered as the yield of each plot. Five plots were used for statistical analyses. Random sampling from the plants grown for yield trials, excluding the edge plants, were performed for scoring average fruit fresh weight per inflorescence, average Brix index per inflorescence and fruit-set rate.

For rice grain-yield evaluation in Beijing paddy fields, three plots were set up, each with an area of ~2 m^2 with plant spacing of 20 cm × 20 cm, a planting density consistent with that of the local farms. Edge plants were included in each plot to avoid edge effects and they were not counted in the total-yield quantification. Excluding the edge plants, each plot had a total of 64 plants, all of which were harvested and dried in a 37°C drying oven. For rice grain-yield evaluation in Hainan paddy fields, 10 plots were set up, each with an area of 50 m^2 and planting 1,326 rice plants. For statistical analysis of the yield data, we randomly reorganized the 10 plots into 5 blocks with two plots for each genotype. Each block covers an area of 100 m^2 and grows 2,652 rice plants, a planting density consistent with that of the local farms. A total of 13,260 plants were planted for each genotype. The harvested rice grains were dried in the sun. The weight of the harvested rice grains was used for grain-yield analysis.

For the sampling type of rice plants in paddy fields in Beijing and Hainan, 6~9 plants, excluding the edge plants, from each plot were randomly selected for scoring tiller number, panicle length, number of primary branches, number of secondary branches, number of grains per panicle, seed-setting rate, 1,000-grain weight, yield per plant and harvest index. The harvest index is defined as the ratio of the total dry weight of the panicle to the total dry biomass weight of the aboveground portion of the plant.

Quantification of tomato sugar contents

Fresh tomato fruits at the 5-DPA stage were collected and ground into a fine powder using liquid nitrogen. Subsequently, the sample powder was completely lyophilized with a lyophilizer (Labconco, FreeZone®). 20 mg of the lyophilized powder was dissolved in 1 mL of chromatography-grade pure water followed by ultrasonic extraction for 30 min. Samples were then centrifuged at 14,000 rpm for 10 min at 4°C in a tabletop microcentrifuge. The filtrate was collected by taking 800 μL of the supernatant and filtering it through a 0.1 μm filter (Syringe Filter, TNL21060727). The filtrate was diluted 40 times with chromatography-grade pure water then loaded into injection-chromatography vials for ion chromatography. A Thermo Scientific Dionex ICS-5000+ ion chromatograph (Thermo Fisher) equipped with a single pump, eluent generator, autosampler, electrochemical detector and Chromeleon7.2 SR5 chromatographic data analysis software was connected to a Dionex CarboPac PA10 BioLC carbohydrate column (analytical column: 4 mm × 250 mm, protective column: 4 mm × 50 mm, Thermo Fisher). The mobile phase comprised buffer A: chromatography-grade pure water and buffer B: 200 mM sodium hydroxide (Sigma, 415413) (prepared diluting 50% NaOH plus chromatography-grade pure water), with a flow rate of 1 mL/min, 10 μL injection volumes, column temperature set to 35°C and sample-chamber temperature set to 8°C.

Phylogenetic and sequence analyses

We used 33 sHSPs reported in tomato as reference,[45] and identified 37 and 32 homologous proteins in *A. thaliana* and *O. sativa* using BLASTP (blast 2.60+) (E-value < 10^{-5} and identity ≥ 30%). The phylogenetic tree was constructed using the maximum likelihood (ML) method in MEGA X.[87] The bootstrap consensus tree was inferred from 100 bootstrap replicates. The promoter sequence of *sHSP* families was obtained from Phytozome v13 (https://phytozome-next.jgi.doe.gov/). To identify the consensus elements for heat-shock elements, promoter sequences located within 1,000 bp upstream of the annotated transcriptional start sites in *Arabidopsis*, rice and tomato were used for motif screening. MEME's motif-discovery function[88] was employed with the specified parameter 'look for palindromes only' (https://meme-suite.org/meme/tools/meme). Sequences with an E-value and hits with a *p*-value were based on default settings.

Constructs, gene editing and plant genotyping

To generate tomato *lin5*^{CR} mutants, gene-specific guide RNAs for targeting *LIN5* exons (Table S5) were designed using the online tool (http://cbi.hzau.edu.cn/cgi-bin/CRISPR). They were constructed into pDIRECT–22C vector[84] using standard Golden Gate assembly. To prepare the construct for over-expression of *LIN5* from the CaMV *35S* promoter (*35S*$_{pro}$*:LIN5*) in stable transgenic plants, the coding sequence of *LIN5* was amplified from c.v. Micro-Tom cDNA and ligated into the pRI101 vector[86] with a ClonExpress II One Step Cloning Kit (Vazyme Biotech, C115).

To develop the prime-editing systems for tomato and rice, modifications were made to the previously reported pDIRECT-22C[84] and pYLCRISPR/Cas9P_{ubi}-H[68] vector backbones, the *M-MLV* reverse transcriptase and *nCas9* (H840A) genes were codon optimized for dicotyledonous and monocotyledonous plants, respectively. We added an SV40 nuclear-localization sequence (NLS) at the N-terminus of nCas9 and the C-terminus of the RT, and inserted a linker composed of 33 amino acids containing the SV40 NLS between nCas9 and the M-MLV RT (hereafter termed NRT). The newly established prime-editing vectors were named Csy4–PE and pCAM–PE, respectively. The pegRNA and nicking sgRNAs sequences for comparison of editing efficiency of U6–PE, tRNA–PE and Csy4–PE at *LIN5* targets were all synthesized by BGI (Beijing, China). Other pegRNAs and nicking sgRNAs were synthesized based on the flanking sequences of *cis*-element insertion sites in the promoter of *FLAVIN MONOOXYGENASE* (*Solyc09g074430*), *GIF1* and 5' UTR of *ERRECTA* (*Solyc08g061560*). They were amplified by KODone (TOYOBO, KMM-101) using specific primers (primer lists are in Table S5) and were cloned into the Csy4–PE and pCAM–PE backbones that digested with BsaI (NEB, R0535L) by in-fusion cloning (Vazyme Biotech, C115). The resulting constructs were transformed into plants by *Agrobacterium*-mediated transformation and tissue-culture protocols as described in ref.[82,83]

First-generation (T_0) transgenic plants were transplanted in soil and grown under standard greenhouse conditions. All mutant alleles used in this study were derived from backcrossing T_0 plants with non-transformed wild-type plants to exclude the influence of genetic background and possible off-target effects on the phenotypic comparison of gene-edited offsprings. CRISPR–Cas9, Csy4–PE and pCAM–PE-induced mutations were genotyped by Ultra Taq PCR StarMix (GenStar, ZA019-101S) using specific primers (primer lists are in Table S5) with XbaI (NEB, R0145) restriction endonuclease validation and Sanger sequencing. Three leaf samples from different parts of each recovered plant were collected and pooled together for DNA extraction using a cetyltrimethylammonium bromide (CTAB)-based method.[99] Gene sequences were obtained from the Sol Genomics Network (SGN) database (https://solgenomics.net/) and the Rice Annotation Project (RAP) database (https://rapdb.dna.affrc.go.jp/).

Prediction of pegRNA spacer-like off-target edits

The pegRNA spacer-like off-target sites were predicted with an offline version of Cas-OFFinder.[89] A maximum of five mismatches were allowed between the on- and off-target sequences.[100] The three top scoring off-target sites were PCR amplified and sequenced. Primers can be found in Table S5.

Prime editing target-region selection and *cis*-element selection

To select insertion sites for the HSE in *CWIN* genes, we first analyzed the *cis*-elements in the promoter regions to avoid the disruption of native *cis*-elements. PlantCARE (http://bioinformatics.psb.ugent.be/webtools/plantcare/html/)[90] was used to identify candidate sites that are predicted to not contain known *cis*-elements. Next, we analyzed the promoter of *CWIN* genes using publicly available high-resolution maps of DNase-I hypersensitive sites from fruit tissues of tomato c.v. Ailsa Craig at 17 and 47 DPA (http://www.epigenome.cuhk.edu.hk/jbrowse2/),[46] by which the sites can be largely avoided. To avoid disruption of gene-expression patterns, regions with weak transcription-factor binding signals and relatively inactive chromatin were selected as candidate targeting sites. When selecting inserted *cis*-element units, three key factors need to be considered: 1. Activity. It is important to ensure that the chosen unit has high activity, without sacrificing effectiveness in pursuit of the shortest size. 2. Insertion efficiency. While ensuring activity, the shorter the insertion sequence, the higher the prime-editing efficiency, at least with current technology. 3. Chromatin maintenance. Generally, shorter knock-in sequences cause less disruption to the chromatin structure of the promoter region, allowing for the maintenance of the target gene's expression pattern with minimal side effects.

Transcriptional activity assays

Dual-luciferase assays were performed as previously reported.[85] Briefly, the *LUCIFERASE* (*LUC*) reporter gene driven by an ~2 kb upstream promoter region of *LIN5* (*$LIN5_{pro}$:LUC*; *$LIN5_{pro+HSE}$:LUC*; *$LIN5_{pro+HSE\ scram}$:LUC*) served as a reporter and the firefly *Renilla* (*REN*) gene driven by CaMV *35S* promoter (*$35S_{pro}$:REN*) was used as an internal control in a *pGreenII0800-LUC* vector backbone.[85] The resulting constructs were co-infiltrated into tobacco leaves (*Nicotiana benthamiana*) and the infiltrated area was marked for subsequent sampling. After propagation for 48 h under normal conditions, tobacco plants were subjected to heat treatment in a growth chamber (40°C for 0.5, 1, 2, 4, 8 h, respectively). A 5 mm diameter punch was used to rapidly sample the different infiltrated areas of the heat-treated leaves, and leaf disks were snap frozen on liquid nitrogen.

The Dual-Glo®Luciferase Assay System (Promega, E1910) was used to measure the LUC and REN activities in accordance with the manufacturer's recommendations. Leaf samples were homogenized and extracted with 100 μL 'Passive Lysis Buffer' followed by 15 min of centrifugation (12,000 rpm) at 4°C. Samples were then prepared for chemiluminescence detection in a GloMax 96 Microplate Luminometer (Promega) with a 2 s delay and a 10 s measurement time for LUC and REN signal determination. Transcriptional activity was reflected by the ratio of LUC to REN.

RNA extraction and quantitative RT–PCR (RT–qPCR)

Total RNA was extracted with TRIZOL reagent (Invitrogen, 15596018) from fresh fruits at 5 DPA under normal and heat-stress conditions. To examine the expression pattern of *LIN5*, contemporaneous roots, stems, leaves, flower buds (4mm), ovaries (flowering stage) and fruits (5 DPA) were sampled. To assess the expression levels of *LIN5* and *GIF1* under heat treatment, we collected samples of tomato fruits and rice grains at 5 DPA following a 1 h exposure to 40°C and 42°C, respectively. Fastking RT Kit (Tiangen, KR116)

Please cite this article in press as: Lou et al., Engineering source-sink relations by prime editing confers heat-stress resilience in tomato and rice, Cell (2025), https://doi.org/10.1016/j.cell.2024.11.005

was used for reverse transcription. RT–qPCR analysis was performed with the TB Green Premix Ex Taq II kit (Takara, RR820) on a CFX96 Real-Time system (Bio-Rad) by following the manufacturer's instructions. PCR reactions were performed in quadruplicate, for each sample, and expression levels were normalized to *Ubiquitin* (tomato) or *Actin* (rice) for calculation of relative expression. The experiments were repeated independently three times. Gene-specific primers are listed in Table S5.

Leaf-level photosynthetic activity measurements

Leaf gas exchange measurements were performed using a LI6800 Portable Photosynthesis System (LiCor, Lincoln, NE, USA). In tomato, the measurements were taken at 9:00-11:00 am and the leaf nearest to the second inflorescence was detected under normal condition and heat stress. For the heat stress treatment, 4-week-old plants were exposed to the condition with day temperature at 40 °C (16 h) and night temperature at 30°C (8 h) for 48 h. Gas exchange parameters, namely net photosynthetic CO_2 uptake rate (A), internal CO_2 concentration (C_i), and stomatal conductance (g_s) were measured using an instrument calibrated to a reference CO_2 concentration of 400 μmol mol^{-1}, a PPFD (photosynthetic photon flux density) of 1500 μmol m^{-2} s^{-1}, a flow rate of 500 μmol s^{-1} and a maintained relative humidity of 60%.

Cytology analysis of microspores and pollen viability determination

To assess microspore development and pollen viability, samples were collected from the flowers on plants grown in commercial solar greenhouse under normal and heat stress conditions. Mature pollen viability was evaluated by staining with Alexander solution.[101] Given microscopes at tetrad stage are most sensitive to temperature changes,[102,103] we therefore performed cytology analysis of tetrad-stage microspores. The collected microspores were fixed in FAA solution and vacuumed for 30 min. Following fixation, the samples were gradually dehydrated through a graded series of ethanol solution (30%, 50%, 70%, 90%, and 100%) for 30 min at each concentration. The dehydrated samples were infiltrated with Technovit®7100 resin (Kulzer, Germany), following the manufacturer's instructions. Briefly, mix ethanol absolute and Technovit 7100 base liquid in equal volumes to prepare the pre-infiltration solution. The samples were placed in the pre-infiltration solution for 2 h. A solution of 100 mL Technovit®7100 base liquid mixed with 1 g of Hardener I were prepared for infiltration. The samples were placed in the infiltration solution and allowed to infiltrate at room temperature for 12 h. The infiltrated samples were transferred into embedding molds and submerged in the resin mixture (1 mL Hardener II + 15 mL of resin solution) for polymerization. After polymerization, the resin blocks were trimmed and sectioned at a thickness of 5 μm using a rotary microtome (LeicaRM2265, Germany). Sections were placed on glass slides for staining using Toluidine Blue and were then observed under a light microscope (LeicaDFC7000T, Germany).

The ^{14}C-labelled sucrose partitioning assay

For measuring source-sink dynamics in tomato, shoot cuttings with inflorescences of c.v. Micro-Tom were obtained from 4-week-old plants. The cuttings about 8 to 10 cm length were placed in beakers containing 7 ml of ^{14}C-labelled sucrose solution (1 μCi ^{14}C-sucrose in 0.05% MES (2-[N-Morpholino] ethanesulfonic acid), pH 5.5). Then, those beakers are covered with clear plastic cups to maintain humidity. The materials were incubated in an artificial climate room (16 h light at 25°C/8 h darkness at 22°C, normal condition) equipped with LED lights at 140 μmol m^{-2} s^{-1} light intensity for 48 h. For heat stress treatment, shoot cuttings soaked in the ^{14}C-labelled sucrose solution were exposed to the condition with day temperature at 40°C (16 h) and night temperature at 30°C (8 h) for 24 h. Following heat treatment, shoot cuttings were allowed to recover under normal condition for 24 h. After the incubation, the leaf nearest to inflorescences were collected and transferred into scintillation fluid to assess ^{14}C radioactive signals in the source organs. The ovaries at similar developmental stages were collected and placed into scintillation fluid to determine ^{14}C radioactive signals in the sink organs. One leaf and five ovaries from each shoot cuttings were set as a replicate for statistical analysis. The ^{14}C radioactive signals were detected using a liquid scintillation counter after 18 h incubation in the scintillation fluid.

Yeast one-hybrid assays

Yeast one-hybrid assays was performed using a Matchmaker™ Gold Yeast One-Hybrid System (Clontech, 630491, 630466, 630499). Briefly, the promoter sequences of $LIN5_{pro\ +\ HSE}$ and $LIN5_{pro\ +\ HSE\ scram}$ were amplified from $LIN5_{pro\ +\ HSE}$:*LUC* and $LIN5_{pro\ +\ HSE\ scram}$:*LUC* vectors, respectively, and cloned into pAbAi vector. The full-length cDNAs of the *HsfA1a*, *A2*, and *A2c* were recombined into the pGADT7 vector respectively, which were used for transformation into Y1H Gold competent cells carrying pAbAi-$LIN5_{pro\ +\ HSE}$ or pAbAi-$LIN5_{pro\ +\ HSE\ scram}$. The yeast cells were screened on selective medium (SD) lacking Leu (SD/-L) supplemented with 150 ng/ml AbA. A total of three independent replications were performed.

Genetic diversity analysis of the *GIF1* locus among elite modern rice varieties

To assess whether the *GIF1* locus has been utilized in breeding in modern elite rice varieties, we selected 16 elite *japonica* varieties with genome data to analysis the genetic variation (Table S4).[67,104–106] The genomic sequences (including 3 kb upstream and gene-body) of *GIF1* from 16 accessions were analyzed using BLASTN (blast 2.60+) with an E-value cutoff of 10^{-5}.[91] These genomic sequences were aligned to the *GIF1* sequence of using mVISTA LAGAN alignment (http://genome.lbl.gov/vista/mvista/submit.shtml).[92] For examination of the sequence diversity around the HSE insertion site, ~230 bp upstream and ~510bp downstream of insertion sites were compared and the consensus sequence was calculated by Jalview software.[93]

The transcriptome analysis

Tomato fruits at 5 DPA were used for transcriptome analysis. Three biological replicates were prepared for c.v Micro-Tom and *lin5-de* grown under normal conditions. Total RNA was extracted using TRIZOL reagent (Invitrogen, 15596018) and contaminating DNA was removed using the TURBO DNA-free Kit (Invitrogen, AM1907). Libraries were prepared and sequenced on Illumina NovaSeq platform. About 22,741,100 ~41,355,217 paired-end reads (150 bp) were generated for each sample. Raw data were filtered using Trimmomatic (v0.36) (ILLUMINACLIP: adapter. fa: 2:30:10 LEADING:20 TRAILING:20 SLIDINGWINDOW: 4:15 MINLEN:36).[94] RNA-seq reads were mapped to the SL4.0 genome (https://solgenomics.net/organism/ Solanum_lycopersicum/genome) using Hisat2 (v2.1.0).[95] Alignments were sorted by samtools (v1.8) software[96] and assembled into transcripts using StringTie (v2.0.3).[97] Statistically significantly differentially expressed genes were calculated with DESeq2 using padj $\leq$ 0.05 and |log2FoldChange| > 1. Gene Ontology enrichment analysis was performed using agriGOV2.0 (http://systemsbiology.cau.edu.cn/ agriGOv2/) with p value < 0.005.[98] Bubble charts were drawn using ggplot2 (https://ggplot2.tidyverse.org).

QUANTIFICATION AND STATISTICAL ANALYSIS

The statistical information for each analysis is provided in the respective figure legends, including the statistical tests used, exact value of sample size (*N*), what *N* represents, definition of center, and dispersion measures. Comparisons for two groups were calculated using the unpaired two-tailed Student's *t* tests, and statistical analysis was performed using Microsoft Excel 2021. Comparisons among various groups were calculated using one-way ANOVA, and statistical analysis was performed using SPSS Statistics. Results are represented as mean ± standard deviation. *P* values are indicated above each bar graph. We observed a normal distribution and found no difference in variance between groups in individual comparisons. The sample size was determined based on extensive experience. Additional methods to assess whether the data met the assumptions of the statistical approach were not relevant for these analyses.

Supplemental figures

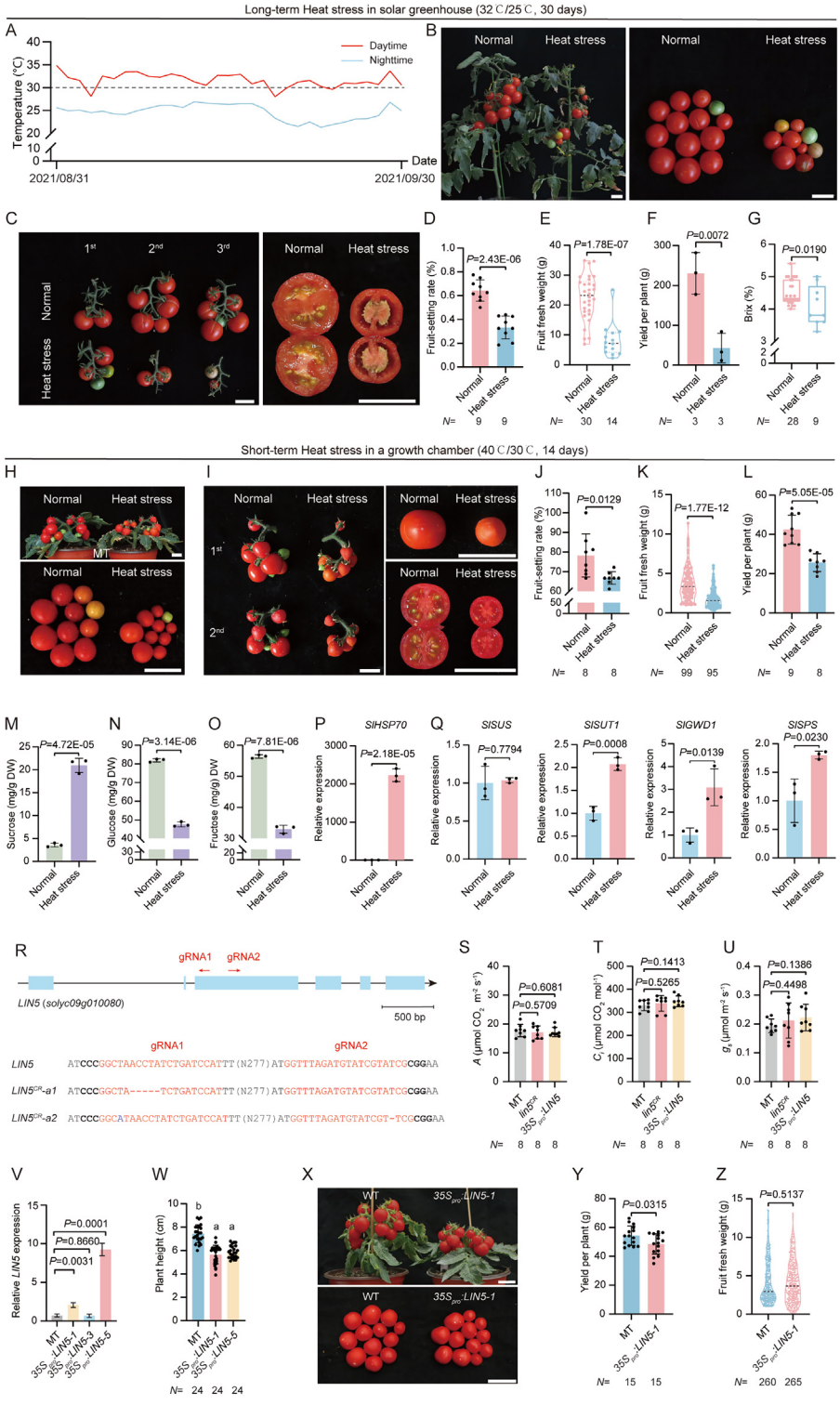

(legend on next page)

Figure S1. Fruit yield analysis of two tomato cultivars Micro-Tom and Ailsa Craig caused by heat stress, as well as in *lin5*^{CR} null mutants and *LIN5* overexpression lines under normal condition, related to Figures 1 and 2

(A) Daytime and nighttime temperature medians every day over a course of 1-month period during the Ailsa Craig growing season in greenhouse. Daytime corresponds to 9 a.m.–6 p.m. during which the greenhouse was supplemented with artificial lighting. The black dashed line indicates 30°C.

(B) Representative phenotypes of Ailsa Craig shoots (left) and total fruits per plant (right) under heat-stress conditions in a greenhouse as described in (A). Scale bars, 3.5 cm.

(C) Representative phenotypes of Ailsa Craig inflorescence (left) and fruit transverse sections (right) under normal and heat-stress conditions in a greenhouse as described in (A). Scale bars, 3.5 cm.

(D–G) Quantification of fruit-setting rate (D), fruit fresh weight (E), yield per plant (F), and sugar content (G) of Ailsa Craig under normal and heat-stress conditions in a greenhouse as described in (A). *N*, individual plant number (D and F), fruit number (E and G). Data are mean ± SD. *p*, two-tailed, two-sample t test.

(H and I) Representative phenotypes of Micro-Tom shoots (H, upper), total fruits per plant (H, lower), inflorescence (I, left), and fruit transverse section (I, right) under normal and heat-stress conditions in growth chamber (40°C/30°C day/night temperatures) for 14 days. Scale bars, 3.5 cm.

(J–L) Quantification of fruit-setting rate (J), fruit fresh weight (K), and yield per plant (L) of Micro-Tom under normal and heat-stress conditions (40°C/30°C day/night temperatures) for 14 days in growth chamber. *N*, individual plant number (J and L), fruit number (K). Data are mean ± SD. *p*, two-tailed, two-sample t test.

(M–O) Quantification of sucrose (M), glucose (N), and fructose (O) contents in fruits at 5 DPA between normal and heat-stress conditions for Ailsa Craig grown in a growth chamber. Data are the mean ± SD, *N* = 3 biological replicates. *p*, two-tailed, two-sample t test.

(P and Q) RT-qPCR analysis of *HSP70* and source-sink-related gene expression in Micro-Tom under normal and heat-stress conditions. Data are the mean ± SD, *N* = 3 biological replicates, and relative expression was normalized to *UBIQUITIN*. *p*, two-tailed, two-sample t test.

(R) Generation of *lin5*^{CR} null mutations by CRISPR-Cas9 using two single-guide RNAs (gRNA1 and gRNA2; red arrows). Sequences of *lin5*^{CR} *allele 1* (*a1*) and *allele 2* (*a2*) are shown beneath that of *LIN5* from wild-type Micro-Tom. sgRNA targets and the protospacer-adjacent motif (PAM) are indicated in red and bold font, respectively, and deletions depicted by red hyphens. Insertions are indicated in blue, and sequence gap length is shown in parentheses.

(S–U) Photosynthesis-parameter measurements in wild-type Micro-Tom, *lin5*^{CR}, and *35S*$_{pro}$*:LIN5* plants. Gas exchange parameters, namely, net photosynthetic CO_2 uptake rate (*A*) (S), internal CO_2 concentration (C_i) (T), and stomatal conductance (g_s) (U) were measured. *N*, individual plant number. Data are mean ± SD. *p*, two-tailed, two-sample t test.

(V) RT-qPCR assay of *LIN5* expression in wild-type Micro-Tom and T_1 *35S*$_{pro}$*:LIN5* stable-transgenic lines. Expression was normalized to *UBIQUITIN*, and data are the mean ± SD of *N* = 3 biological replicates. *p*, two-tailed, two-sample t test.

(W) Quantification of plant height for wild-type Micro-Tom and T_1 *35S*$_{pro}$*:LIN5-1* and *35S*$_{pro}$*:LIN5-5* transgenic lines. *N*, number of plants. *p*, two-tailed, two-sample t test. Each value represents the mean ± SD (*N* = 24). Means with different letters are significantly different ($p < 0.05$, ANOVA).

(X) Representative phenotypes of shoots (upper) and total fruits per plant (lower) for wild-type Micro-Tom and *35S*$_{pro}$*:LIN5-1* grown in a growth chamber under normal conditions. Scale bars, 3.5 cm.

(Y and Z) Quantification of yield per plant (Y) and fruit fresh weight (Z) in wild-type Micro-Tom and *35S:LIN5-1*. *N*, individual plant number (Y), fruit number (Z). Data are mean ± SD. *p*, two-tailed, two-sample t test.

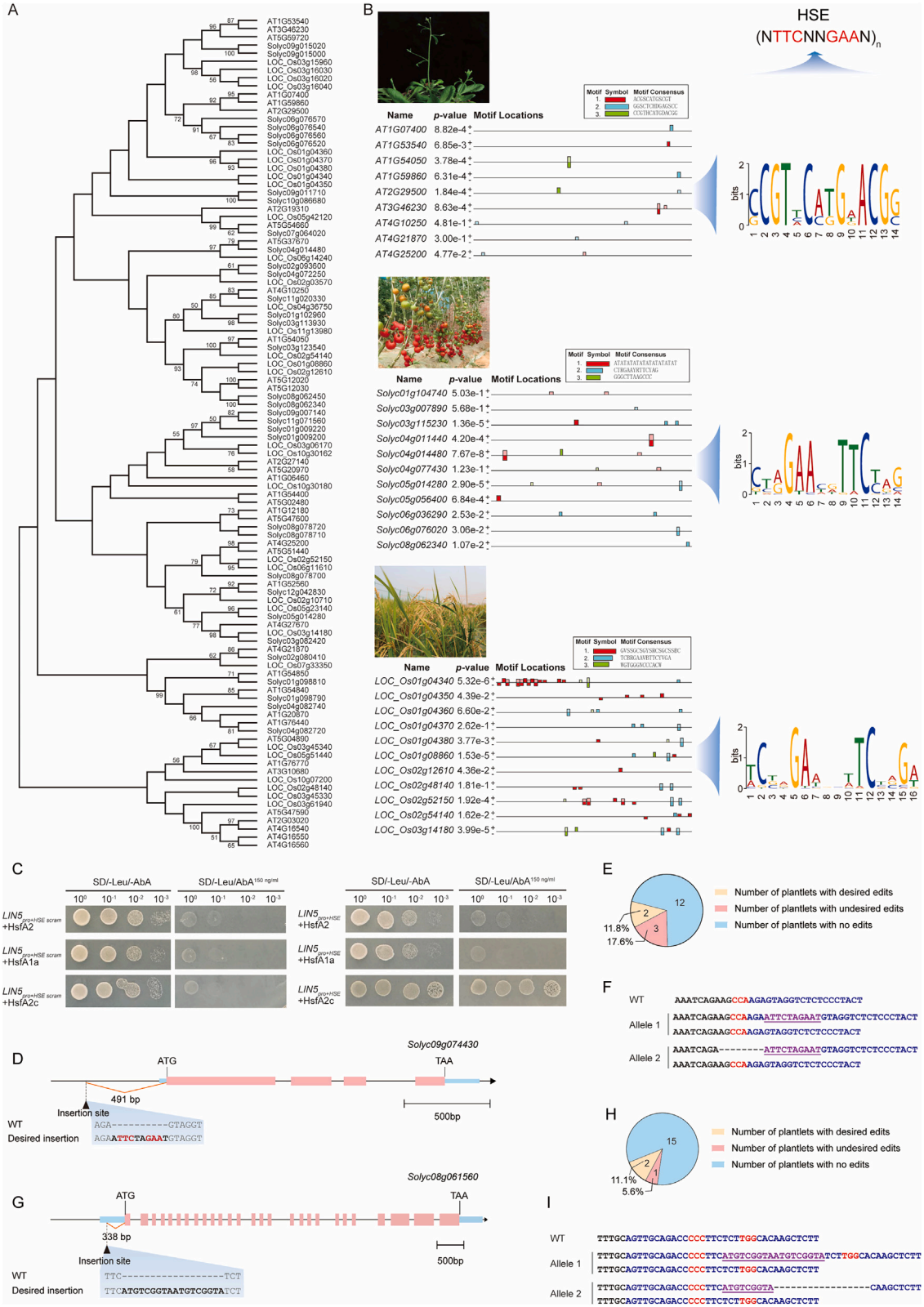

(legend on next page)

Figure S2. Heat-shock elements analysis across diverse angiosperms and prime-editing efficiency comparison at different loci of different genes, related to Figure 3

(A) Phylogenetic tree of annotated sHSP across different plant species using MEGA with 100 bootstraps.

(B) Motif analysis with 1-kb promoter sequences located upstream of the annotated translational start codon of heat-stress-related genes in *Arabidopsis*, rice, and tomato, multiple em for motif elicitation (MEME)'s motif-discovery function was employed for motif screening, with the specified parameters "motif sites can appear multiple times in each sequence," "the maximum and minimum width of motif are 6 and 20, respectively," and "look for palindromes only." A consensus heat-shock element was then obtained (bottom).

(C) Yeast one-hybrid assays showing tomato HsfA2c and HsfA2 bind to the HSE present in the *LIN5* promoters. SD/−Leu/−AbA represents non-selective medium minus Leu and Aureobasidin A (AbA); SD−Leu/AbA 150 ng/mL represents selective medium minus Leu supplemented with 150 ng/mL AbA. The transformants grow on SD/−Leu/AbA 150 ng/mL medium with gradient dilution (1, 1/10, 1/100, and 1/1,000). These assays were repeated three times with similar results.

(D) Illustration of an HSE element inserted into the *FLAVIN MONOOXYGENASE* promoter.

(E) Frequencies of prime editing induced by Csy4-PE in regenerated tomato plantlets.

(F) Sequences of different prime-edited *FLAVIN MONOOXYGENASE* alleles. Guide RNA and PAM sequences are highlighted in blue and red; inserted sequences are highlighted in purple and bold underlined, respectively. Black dashes indicate deletions.

(G) Illustration of a *cis*-element inserted into the *ERECTA* 5′ UTR. Blue boxes indicate indicates 3′ or 5′ UTR.

(H) Frequencies of prime editing induced by Csy4-PE in regenerated tomato plantlets.

(I) Sequences of different prime-edited *ERECTA* alleles. Guide RNA and PAM sequences are highlighted in blue and red; inserted sequences are highlighted in purple and bold underlined, respectively. Black dashes indicate deletions.

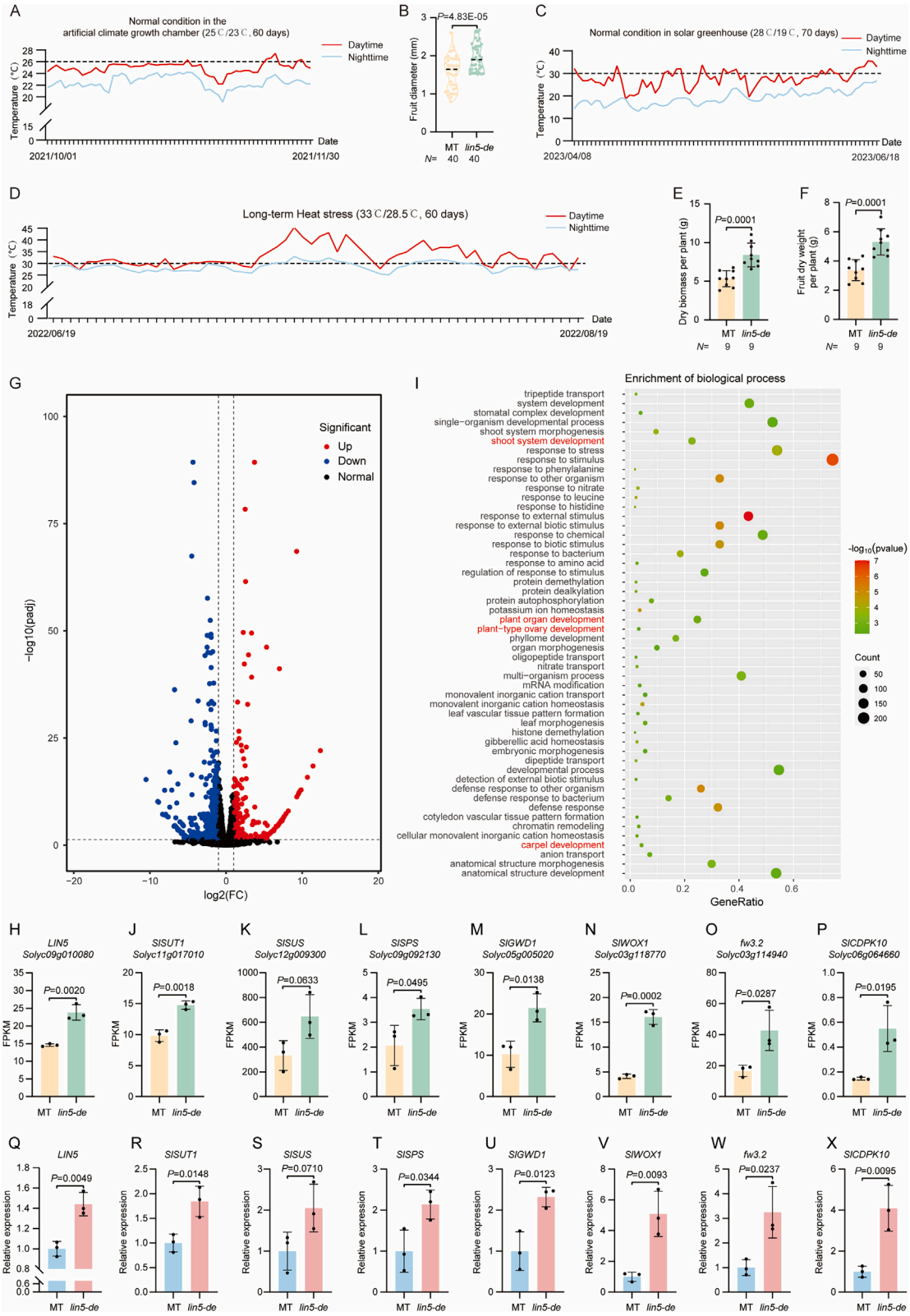

(legend on next page)

Figure S3. RNA-seq analysis of Micro-Tom versus *lin5-de* under normal conditions and RT-qPCR validation, related to Figure 4

(A) Daytime and nighttime temperature medians of every day over a course of 60 days period of growing season under normal conditions in growth chamber. The black dashed line indicates 26°C.

(B) Quantification of fruit diameter in Micro-Tom and *lin5-de* under normal conditions in commercial greenhouse. *N*, number of fruits. Data are mean ± SD. *p*, two-tailed, two-sample t test.

(C) Daytime and nighttime temperature medians of every day over a course of 70 days period of growing season under normal conditions in commercial greenhouse. The black dashed line indicates 30°C.

(D) Daytime and nighttime temperature medians of every day over a course of 60 days period of growing season under long-term heat stress conditions in commercial greenhouse. The black dashed line indicates 30°C.

(E and F) Quantification of dry biomass per plant (E) and fruit dry-weight per plant (F) in Micro-Tom and *lin5-de* under normal conditions in commercial greenhouse. *N*, number of plants. Data are mean ± SD. *p*, two-tailed, two-sample t test.

(G) Volcano plot of Micro-Tom and *lin5-de* gene-expression differences greater or less than 2-fold.

(H) RNA-seq reveals relative expression levels of gene *LIN5* in Micro-Tom and *lin5-de* under normal conditions in growth chamber.

(I) Gene Ontology enrichment for upregulated genes in *lin5-de* relative to Micro-Tom. See also Table S3.

(J–P) RNA-seq reveals relative expression of *SlSUT1* (J), *SlSUS* (K), *SlSPS* (L), *SlGWD1* (M), *SlWOX1* (N), *fw3.2* (O), and *SlCDPK10* (P) in Micro-Tom and *lin5-de*.

(Q–X) RT-qPCR analysis of *LIN5* (Q), *SlSUT1* (R), *SlSUS* (S), *SlSPS* (T), *SlGWD1* (U), *SlWOX1* (V), *fw3.2* (W), and *SlCDPK10* (X) in Micro-Tom and *lin5-de*. Data are the mean ± SD, *N* = 3 biological replicates, and relative expression was normalized to *UBIQUITIN*.

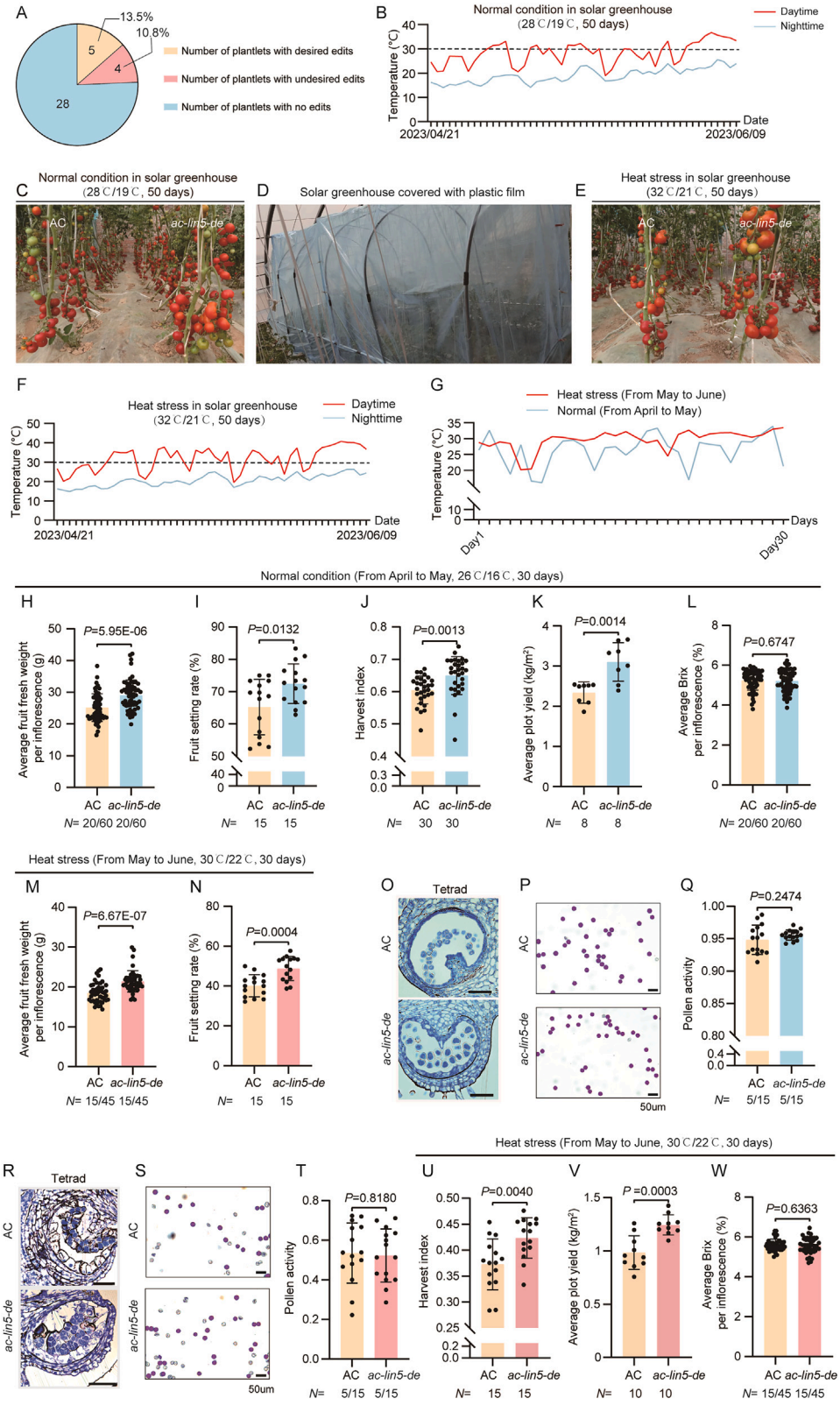

(legend on next page)

Figure S4. Growth conditions and phenotypic analysis of Ailsa Craig and *ac-lin5-de* plants under different seasons and locations, related to Figure 5

(A–F) Characterization of growth conditions in the greenhouse and open field for propagation of Ailsa Craig and *ac-lin5-de* plants.

(A) Summary of prime editing induced by Csy4-PE in 37 regenerated tomato plantlets in the Ailsa Craig background.

(B) Daytime and nighttime temperature medians during the reproductive growth period under normal conditions in the greenhouse. The black dashed line indicates 30°C.

(C) Representative whole-view image of tomato populations under normal conditions in the greenhouse.

(D) Plastic film covering tomato plants in the greenhouse to create heat-stress condition.

(E) Representative whole-view image of tomato populations grown under the high-temperature regime in the greenhouse covered with plastic film as shown in (D).

(F) Daytime and nighttime temperature medians during the reproductive growth period under heat-stress conditions in the greenhouse. The black dashed line indicates 30°C.

(G) Daytime temperature medians during the growth period in the plastic solar greenhouse in different season and location. The blue line indicates normal conditions, and the red line indicates higher temperature conditions.

(H–N) Quantification of average fruit fresh weight per inflorescence (H and M), fruit-setting rate (I and N), harvest index (J), average plot yield (K), and average Brix per inflorescence (L) of Ailsa Craig and *ac-lin5-de* grown in plastic solar greenhouse under normal conditions (H–L) and heat stress (M and N). *N*, number of plants and inflorescences (H, L, and M), individual plant number (I, J, and N), yield plot number (K). Data are mean ± SD. *p*, two-tailed, two-sample t test.

(O–Q) Representative images of microspores at the tetrad stage (O), mature pollen (P), and pollen vitality quantification (Q) in Ailsa Craig and *ac-lin5-de* under normal conditions. Scale bars, 50 μm. *N*, number of plants and visual fields. Data are mean ± SD. *p*, two-tailed, two-sample t test.

(R–T) Representative images of microspores at the tetrad stage (R), mature pollen (S), and pollen vitality quantification (T) in Ailsa Craig and *ac-lin5-de* under heat stress. Scale bars, 50 μm. *N*, number of plants and visual fields. Data are mean ± SD. *p*, two-tailed, two-sample t test.

(U–W) Quantification of harvest index (U), average plot yield (V), and average Brix per inflorescence (W) of Ailsa Craig and *ac-lin5-de* grown in plastic solar greenhouse under heat stress. *N*, number of plants and inflorescences (W), individual plant number (U), yield plot number (V). Data are mean ± SD. *p*, two-tailed, two-sample t test.

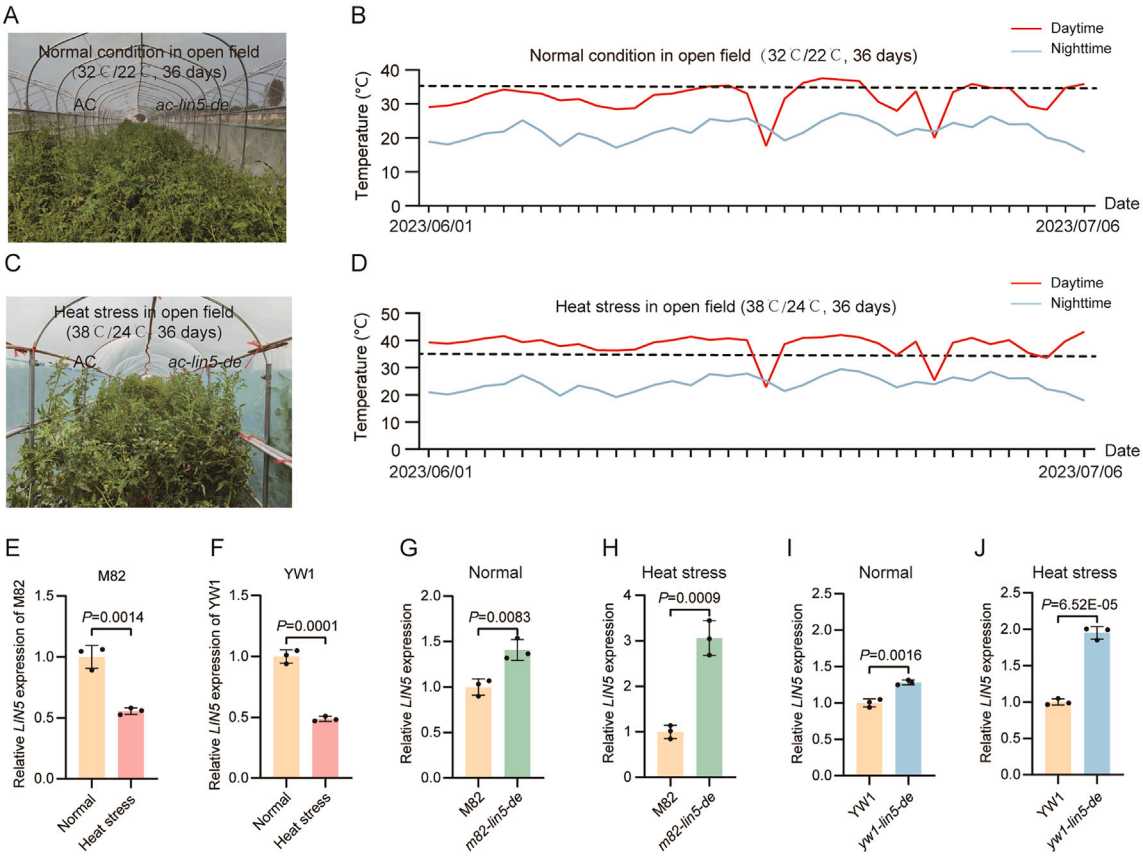

Figure S5. Growth conditions in the open field and RT-qPCR analysis of *LIN5* expression in different tomato varieties, related to Figure 5

(A) Representative whole-view image of tomato populations under open-field conditions covered with insect-proof netting.

(B) Daytime and nighttime temperature medians during the reproductive growth period in the open field covered with insect-proof netting. The black dashed line indicates 35°C.

(C) Representative phenotypes of tomato populations under open-field conditions covered with plastic film to create high-temperature stress condition.

(D) Daytime and nighttime temperature medians during the reproductive growth period in the field covered with plastic film to induce high-temperature stress. The black dashed line indicates 35°C.

(E and F) RT-qPCR analysis of *LIN5* expression in ovaries of flowers exposed to normal conditions or heat stress (40°C) for 1 h in wild-type M82 (E) and YW1 (F). Data are the mean ± SD of *N* = 3 biological replicates, and relative expression was normalized to *UBIQUITIN*.

(G and H) RT-qPCR analysis of *LIN5* expression in ovaries exposed to normal conditions (G) or heat stress (40°C) (H) for 1 h in M82 and *m82-lin5-de*. Data are the mean ± SD of *N*= 3 biological replicates, and relative expression was normalized to *UBIQUITIN*.

(I and J) RT-qPCR analysis of *LIN5* expression in ovaries exposed to normal conditions (I) or heat stress (40°C) (J) for 1 h in YW1 and *yw1-lin5-de*. Data are the mean ± SD of *N* = 3 biological replicates, and relative expression was normalized to *UBIQUITIN*.

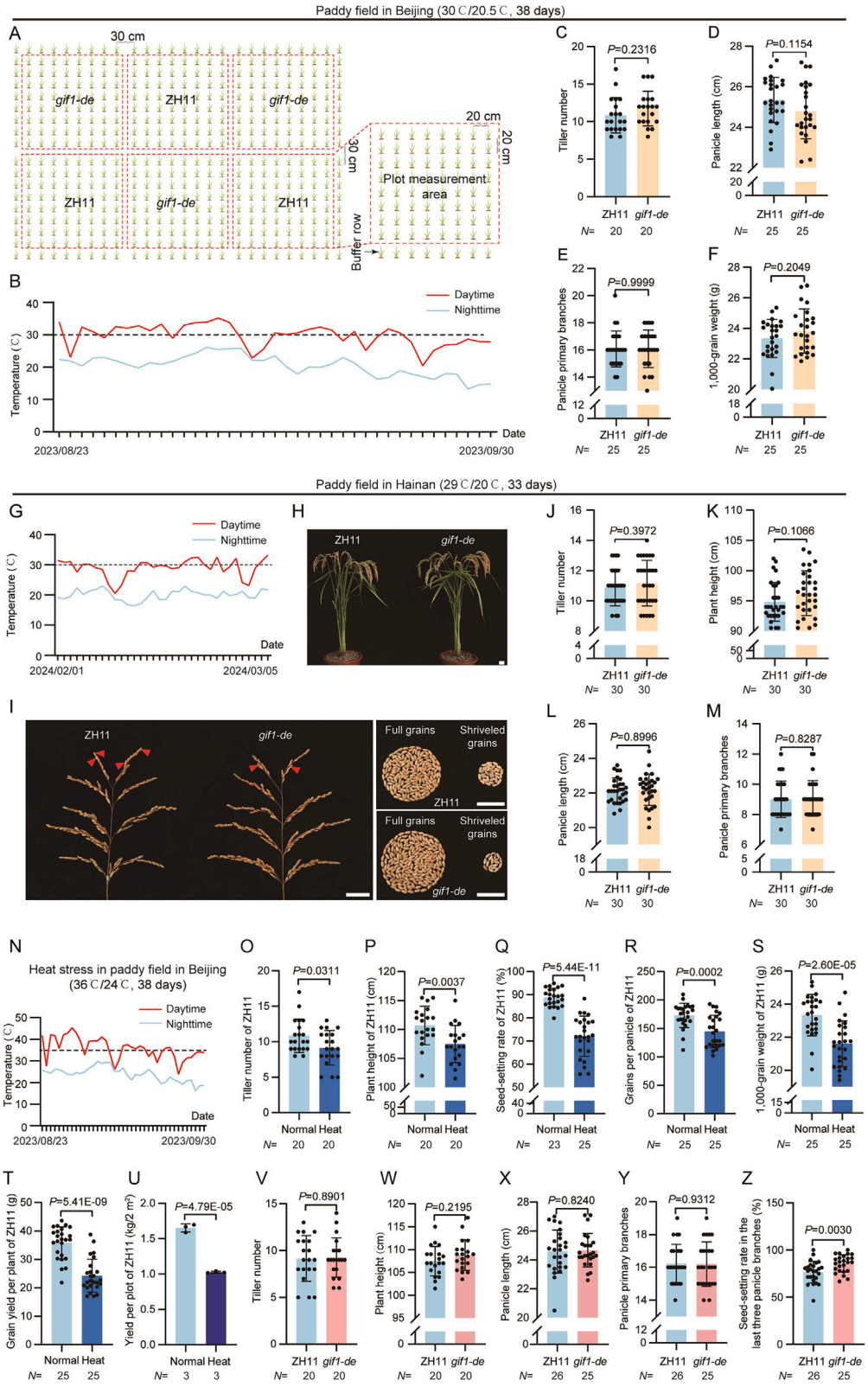

(legend on next page)

Figure S6. Yield-trial design, temperature-monitoring data, and representative phenotypes for rice grown in the paddy field under normal conditions and heat stress, related to Figures 6 and 7

(A) Diagram of rice plots in Beijing. Inside each red dotted box is the actual quantified production area of each genotype, and outside the red dotted line box is the buffer row of plants that were not scored to mitigate edge effects.

(B) Daytime and nighttime temperature medians during the reproductive growth period under normal conditions in the paddy field in Beijing. The black dashed line indicates 30°C.

(C–F) Quantification of tiller number (C), panicle length (D), number of panicle primary branches (E), and 1,000-grain weight (F) in wild-type ZH11 and *gif1-de* under normal conditions in the paddy field in Beijing. *N*, individual plant number (C and F), panicle number (D and E). Data are mean ± SD. *p*, two-tailed, two-sample t test.

(G) Daytime and nighttime temperature medians during the reproductive growth period under normal conditions in the paddy field in Hainan. The black dashed line indicates 30°C.

(H–I) Representative phenotypes of shoots (H), panicles (I, left), and total grains per panicle (I, right) of ZH11 and *gif1-de* under normal conditions grown in the field (29°C/20°C day/night temperatures during heading and grain filling stages) in Hainan. In (I), red arrows indicate empty and aborted grains. Scale bars, 3.5 cm.

(J–M) Quantification of tiller number (J), plant height (K), panicle length (L), and number of primary branches (M) in ZH11 and *gif1-de* under normal conditions in the field in Hainan. *N*, individual plant number (J and K), panicle number (L and M). Data are mean ± SD. *p*, two-tailed, two-sample t test.

(N) Daytime and nighttime temperature medians during the growing period under heat-stress conditions in the paddy field covered with plastic film. The black dashed line indicates 35°C.

(O–U) Comparison of tiller number (O), plant height (P), seed-setting rate (Q), number of grains per panicle (R), 1,000-grain weight (S), yield per plant (T), and yield per plot (U) in c.v. ZH11 grown under normal and heat-stress conditions. *N*, individual plant number (O, P, Q, S, and T), panicle number (R), and yield plot number (U). Data are mean ± SD. *p*, two-tailed, two-sample t test.

(V–Z) Quantification of tiller number (V), plant height (W), panicle length (X), number of panicle primary branches (Y), and seed-setting rates in the last three panicle branches (Z) in wild-type ZH11 and *gif1-de* under heat-stress conditions in the paddy field covered with plastic film. *N*, individual plant number (V and W), panicle number (X, Y, and Z). Data are mean ± SD. *p*, two-tailed, two-sample t test.

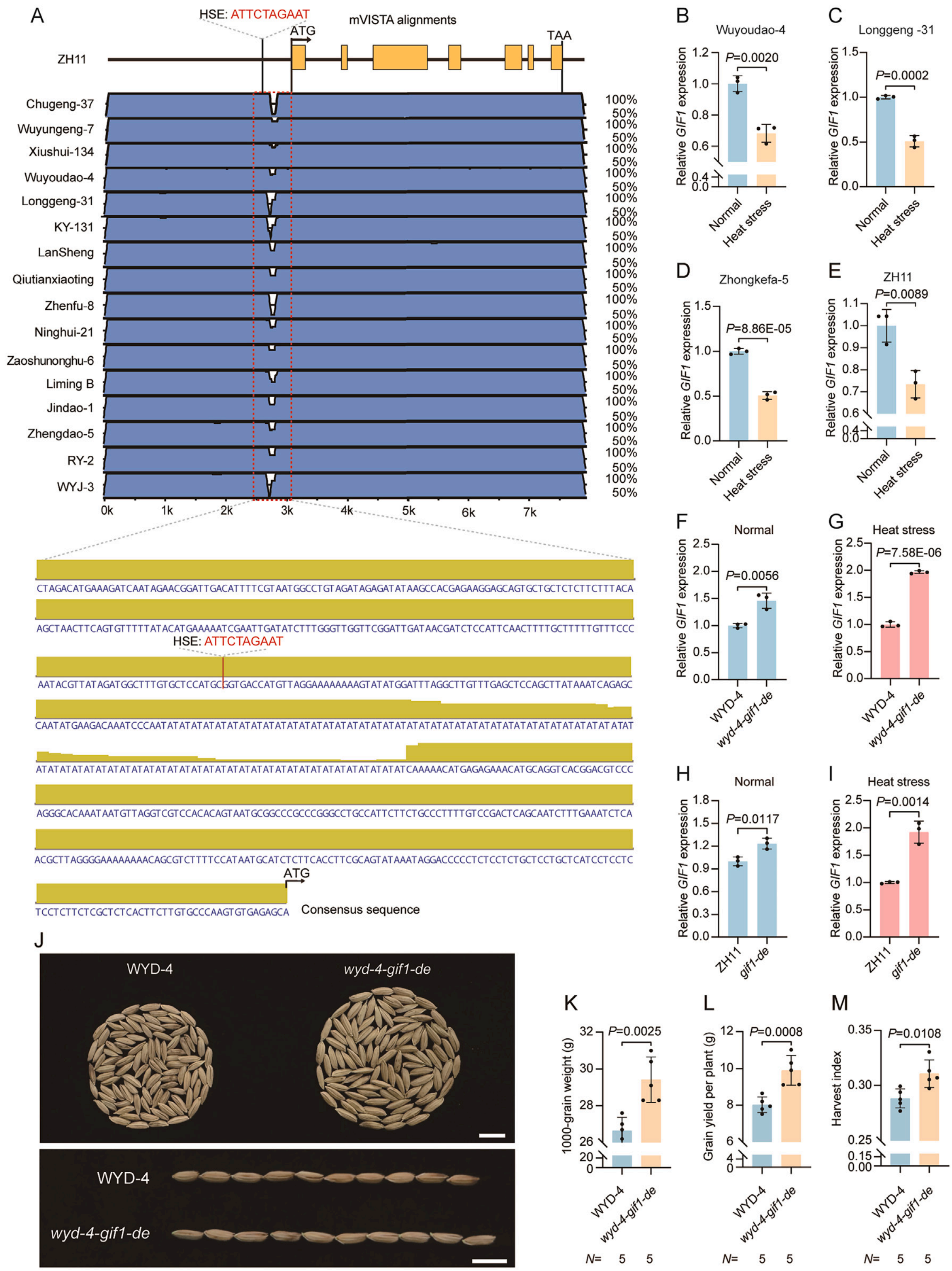

Figure S7. Rational manipulation of *GIF1* expression by CROCS offers an efficient approach for exploiting its potential in crop improvement, related to Figures 6 and 7

(A) Alignment analysis of full-length genomic sequences of *GIF1* from 16 modern elite *japonica* accessions with ZH11. The plots show alignment windows of 100 bp at a similarity threshold of 70% (blue color). The upstream and downstream flanking sequences (~100 bp) around the HSE insertion sites are highly conserved. The consensus sequence is displayed below the alignment. The bar chart shows the percentage of every base, highlighted in yellow.

(legend continued on next page)

(B–E) The *GIF1* expression in Wuyoudao-4 (B), Longgeng-31 (C), Zhongkefa-5 (D), and ZH11 (E) under normal and heat stress conditions. Data are the mean ± SD of *N* = 3 biological replicates, and relative expression was normalized to *ACTIN*.
(F and G) The *GIF1* expression in prime edited *wyd-4-gif1-de* plants under normal (F) and heat-stress conditions (G). Data are the mean ± SD of *N* = 3 biological replicates, and relative expression was normalized to *ACTIN*.
(H and I) The *GIF1* expression in wild-type ZH11 and *gif1-de* plants under normal (H) and heat-stress conditions (I). Data are the mean ± SD of *N* = 3 biological replicates, and relative expression was normalized to *ACTIN*.
(J) Representative phenotypes of 100-grains (upper) and 10-grain length (lower) of WYD-4 and *wyd-4-gif1-de* in the paddy field. Scale bar, 1 cm.
(K–M) Comparison of 1,000-grain weight (K), yield per plant (L), and harvest index (M) in WYD-4 and *wyd-4-gif1-de* plants. *N*, individual plant number. Data are mean ± SD. *p*, two-tailed, two-sample t test.